

1

2 **Sensitivity of the WRF-Chem v4.4 ozone, formaldehyde, and their precursors**
3 **simulations to multiple bottom-up emission inventories over East Asia during the**
4 **KORUS-AQ 2016 field campaign**

5

6 Kyoung-Min Kim¹, Si-Wan Kim^{2*}, Seunghwan Seo¹, Donald R. Blake³, Seogju Cho⁴,
7 James H. Crawford⁵, Louisa Emmons⁶, Alan Fried⁷, Jay R. Herman^{8,9}, Jinkyu Hong¹,
8 Jinsang Jung¹⁰, Gabriele Pfister⁶, Andrew J. Weinheimer⁶, Jung-Hun Woo¹¹, and Qiang
9 Zhang¹²

10

11 ¹Department of Atmospheric Sciences, Yonsei University, Seoul, South Korea

12 ²Irreversible Climate Change Research Center, Yonsei University, Seoul, South Korea

13 ³Department of Chemistry, University of California at Irvine, Irvine, CA, US

14 ⁴Seoul Metropolitan Government Research Institute of Public Health and
15 Environment, Gyeonggi-do, South Korea

16 ⁵NASA Langley Research Center, Hampton, VA, US

17 ⁶National Center for Atmospheric Research, Boulder, CO, US

18 ⁷Institute of Arctic and Alpine Research, University of Colorado, Boulder, CO, US

19 ⁸NASA Goddard Space Flight Center, Greenbelt, MD, US

20 ⁹University of Maryland Baltimore County, Baltimore, MD, USA

21 ¹⁰Korea Research Institute of Standards and Science, Daejeon, South Korea

22 ¹¹Department of Advanced Technology Fusion, Konkuk University, Seoul, South
23 Korea

24 ¹²Department of Earth System Science, Tsinghua University, Beijing, China

25

26

27 *To whom correspondence should be addressed. E-mail: siwan.kim@yonsei.ac.kr

28

29 Date: ~~126/21~~10121/2023

1 Abstract

2 In this study, the WRF-Chem v4.4 model was utilized to evaluate the sensitivity of O₃
3 simulations with different three bottom-up emission inventories (EDGAR-HTAP v2,
4 v3, and KORUS v5) using surface and aircraft data in East Asia during the Korea-
5 United States Air Quality (KORUS-AQ) campaign period in 2016. All emission
6 inventories were found to reproduce the diurnal variations of O₃ and its main precursor
7 NO₂, which is one of the major precursors of O₃, as compared to the surface monitor
8 data. However, the spatial distributions of the daily maximum 8-hour average (MDA8)
9 O₃ in the model do not completely align with the observations. The model MDA8 O₃
10 had a negative (positive) bias north (south) of 30°N over China. All simulations
11 underestimated the observed CO by 50-60% over China and South Korea. In the Seoul
12 Metropolitan Area (SMA), EDGAR-HTAP v2, v3, and KORUS v5 simulated the
13 vertical shapes and diurnal patterns of O₃ and other precursors effectively, but the model
14 underestimated the observed O₃, CO and HCHO concentrations. Notably, the model
15 aromatic VOCs were significantly underestimated with the three bottom-up emission
16 inventories, although the KORUS v5 shows improvements. The model isoprene (ISO)
17 estimations had a positive bias relative to the observations, suggesting that the Model
18 of Emissions of Gases and Aerosols from Nature (MEGAN) version 2.04 overestimated
19 ~~isoprene~~ isoprene ISO emissions. Additional model simulations were conducted by
20 doubling CO and VOC emissions over China and South Korea to investigate the causes
21 of the model O₃ biases and the effects of the long-range transport on the O₃ over South
22 Korea. The doubled CO and VOC emission simulations improved the model O₃
23 simulations for the local emission dominant case, but led to the model O₃

- 1 overestimations for the transport dominant case, which emphasizes the need for
- 2 accurate representations of the local VOC emissions over South Korea.

1 **1. Introduction**

2 Air pollutants not only harm human health but also affect radiative balance, resulting
3 in climate change (Anenberg et al., 2018; Franklin et al., 2015; Lee et al., 2014;
4 Manning and von Tiedemann, 1995; Rosenzweig et al., 2008; Wild et al., 2001).
5 Anthropogenic activities are the primary source of air pollutant emissions, which have
6 significant temporal and spatial variability. Chemical transport models (CTMs) use
7 bottom-up emission data to simulate ambient concentrations of air pollutants. CTMs
8 then process these emissions, tracking their impact through chemistry, transport, and
9 loss through deposition (Zhong et al., 2016). Therefore, sensitivity evaluations of CTMs
10 to anthropogenic emission data are an essential part of atmospheric modeling research.

11 Several bottom-up emission inventories are available for chemical modeling of
12 Asia, including the Multi-resolution Emission Inventory for China (MEIC), Regional
13 Emission inventory in Asia (REAS), and Emissions Database for Global Atmospheric
14 Research-Hemispheric Transport of Air Pollution (EDGAR-HTAP). Since 2010,
15 Tsinghua University has developed the high-resolution MEIC emission inventory for
16 China and updated the data to the v1.3, providing anthropogenic emissions by sector
17 and species from 2008 to 2017 (Zheng et al., 2018). REAS provides emission data in
18 Asia from 1950 to 2015 (Kurokawa and Ohara, 2020). In Europe, EDGAR-HTAP has
19 been developed and widely used for CTM simulations from global to regional scale
20 (Kim et al., 2021; Sharma et al., 2017; Sicard et al., 2021). Recently, EDGAR-HTAP
21 v3 has been published, covering 19 years from 2000 to 2018 compared to only two
22 years (2008 and 2010) in the version 2 data (Crippa et al., 2023). Zhong et al. (2016)
23 compared REAS with EDGAR in July, 2007 over China, while Saikawa et al. (2017)
24 compared 5 emission inventories including REAS, EDGAR, MEIC in China, without

1 validation. As bottom-up emission inventories are continuously updated for recent years,
2 there is an ongoing need to evaluate new emissions data.

3 The Ministry of Environment (MOE) in South Korea and National Aeronautics and
4 Space Administration (NASA) in the U.S. conducted the Korea-United States Air
5 Quality (KORUS-AQ) campaign in May-June 2016. The campaign provided a variety
6 of data sets, including ground-based and airborne observations, useful for the validation
7 of model simulations. The KORUS emissions, developed by Konkuk University, were
8 used by many modeling teams to simulate the air pollutant concentrations during the
9 campaign period. Numerous modeling studies wereare conducted forduring this period
10 including validations of CTM results with diverse observation datasets. Miyazaki et al.
11 (2019) adjusted emission inventories using various satellite data sets and Model for
12 Interdisciplinary Research on Climate with chemistry (MIROC-Chem), resulting
13 improved simulations of tropospheric O₃. Goldberg et al. (2019) reported
14 underestimations of NO_x emissions in South Korea, particularly in Seoul. Souri et al.
15 (2020) also revealed the same issue in South Korea and conducted analysis of the
16 sensitivity of O₃ formation to adjustments in NO_x and volatile organic compound (VOC)
17 emission derived from inverse modeling. Tang et al. (2019) revealed negative biases of
18 simulated CO concentrations in East Asia by utilizing satellite data and the Community
19 Atmosphere Model with Chemistry (CAM-Chem). Choi et al. (2022) modified
20 anthropogenic VOC emissions through the inverse modeling using satellite HCHO
21 observations with the Goddard Earth Observing System with Chemistry (GEOS-Chem),
22 which reduced O₃ and HCHO biases.

23 NowRecently, the most-updated version of bottom-up emission inventories and
24 CTMs have become available for the air pollution modeling studies in East Asia. Earlier

1 ~~research pointed out the prevailing issues associated with diverse bottom-up emission~~
2 ~~inventories.~~ In this study, we selected the EDGAR-HTAP versions 2 ~~and~~ 3, and
3 KORUS version 5 emission data and used the Weather Research and Forecasting model
4 coupled with Chemistry (WRF-Chem) version 4.4 for intercomparison of the three
5 emissions data sets, ~~aiming to elucidate the potential issues~~ understand the status of ~~of~~
6 ~~precursor emissions from bottom-up emission inventories and their uncertainties, which~~
7 ~~that may could impact the O₃ formations in the model.~~ ~~Our analysis focused on~~ O₃ and
8 its major precursors ~~were selected~~ ~~were selected~~ for model evaluation and the model
9 results were ~~evaluated~~ ~~validated~~ with surface observation data in China and South
10 Korea and aircraft data acquired over the South Korean peninsula and surrounding
11 waters.

12 The manuscript is organized as follows. The data and methods section introduces
13 emission inventories, the numerical model, and meteorological and chemical
14 observations. The results section evaluates the model's meteorology and chemistry
15 using routine surface observations over China and South Korea. Subsequently, the
16 model results employing three bottom-up emission inventories are compared with
17 sophisticated chemical observations obtained during the KORUS-AQ field campaign,
18 primarily over South Korea. This comparison summarized the model's performance
19 with each emission inventory. In the discussion section, strategies to enhance surface
20 O₃ simulations, along with accurate precursor simulations, are proposed based on
21 various emission scenarios for urban and regional areas over China and South Korea.
22 The summary and conclusion section follow, providing overview of the key findings
23 and conclusions drawn from the study.

24

1 **2. Data and Methods**

2 **2.1. WRF-Chem model configurations**

3 In this study, we utilized the WRF-Chem v4.4, which was developed by the National
4 Oceanic and Atmospheric Administration (NOAA) and National Center for
5 Atmospheric Research (NCAR), to simulate meteorological variables and chemical
6 species in the atmosphere (Grell et al., 2005). The WRF-Chem v4.4 includes N_2O_5
7 heterogeneous chemistry that consists of several chemical reactions related with ClNO_2
8 and N_2O_5 reactions, resulting in nitrate aerosol. The reactions are incorporated in
9 Secondary Organic Aerosol-Volatility Basis Set (SOA-VBS) with Regional
10 Atmospheric Chemistry Mechanism (RACM) chemistry option (chem = 108) in WRF-
11 Chem (Li et al., 2016).

12 We set 59 vertically customized eta (η) levels as vertical layers. The model's first
13 layer height is approximately 40 m above ground level for the entire domain. The
14 model's vertical layers are designed to include about 17 layers under 1.5 km to simulate
15 planetary boundary layer chemistry and near surface vertical distribution in detail. The
16 horizontal resolution is $28 \times 28 \text{ km}^2$. The simulations in this study start at 12 UTC on
17 April 24 and end at 12 UTC on June 11. The model meteorology restarts every 12 UTC
18 (9 PM local time in South Korea) to minimize numerical errors. After the first 7 days
19 of model initiation (spin-up), we analyzed the model results from May 1 to June 10. We
20 used China standard time (+8 UTC) and Korea standard time (+9 UTC) for evaluations
21 with observations. The model physics, chemistry, and aerosol schemes are summarized
22 in Table S1 with corresponding references. The Global Forecast System (GFS) Final
23 (FNL) analysis data are used for meteorological input and boundary conditions. The
24 Community Atmosphere Model with Chemistry (CAM-Chem) output is used for

1 chemical boundary conditions ([https://www.aocom.ucar.edu/cam-chem/cam-](https://www.aocom.ucar.edu/cam-chem/cam-chem.html)
2 [chem.htmlhttps://rda.ucar.edu/datasets/ds313.7/](https://rda.ucar.edu/datasets/ds313.7/)) (Buchholz et al., 2019; Emmons et al.,
3 2020). We used the Model of Emissions of Gases and Aerosols from Nature (MEGAN)
4 v2.04 to calculate biogenic emissions (Guenther et al., 2006). We did not account for
5 fire emissions because of small impact on air quality simulations during the KORUS-
6 AQ campaign period ([Park et al., 2021](#)). [In our sensitivity simulation with the Fire](#)
7 [INventory from NCAR \(FINN\) v2.5 fire emissions \(Wiedinmyer et al., 2022\), a](#)
8 [marginal increase in the simulated averaged daily maximum 8-hour average \(MDA8\)](#)
9 [O₃ of approximately 1 ppbv \(1.6 %\) was noted in China \(Park et al., 2021\)\(Supporting](#)
10 [information, Figure S1\).](#)

12 **2.2. The model simulations using different anthropogenic emissions**

13 **2.2.1. Bottom-up emission data**

14 EDGAR-HTAP v2, v3, and KORUS v5 [anthropogenic bottom-up emissions inventories](#)
15 are compared with respect to their spatial distribution and total amount in Figure 1 and
16 Table [S23](#). We applied the same diurnal factor for all three emissions data by species,
17 following the diurnal patterns for the Los Angeles Basin as in Kim et al. (2016) (also
18 see Figure [S24](#)).

19 EDGAR-HTAP v2 provides 2-dimensional emissions of CH₄, CO, SO₂, NO_x (NO
20 + NO₂), [total](#) non-methane volatile organic compound (NMVOC), NH₃, PM₁₀, PM_{2.5},
21 BC, and OC in 2008 and 2010 with a horizontal resolution of 0.1° x 0.1°. We used 2010
22 data since it is the most recent data available. The data are partitioned by each sector
23 and its sources such as air, ships, energy, industry, transport, residential, and agriculture

1 (https://edgar.jrc.ec.europa.eu/dataset_htap_v2). For East Asia, it included data from
2 the Model Inter-Comparison Study for Asia (MICS-Asia) and REAS v2.1. In South
3 Korea, it adopted data from the Clean Air Policy Support System (CAPSS) (Janssens-
4 Maenhout et al., 2015), and the underlying emission data had an original horizontal
5 resolution of 0.25° x 0.25° over East Asia, which is resampled to 0.1° x 0.1° resolution
6 by raster resampling and aggregation. The ~~specifically mapped~~ speciated EDGAR-
7 HTAP v2 VOC data were obtained through the WRF-Chem site
8 (<https://www.acom.ucar.edu/wrf-chem/download.shtml>) in the *anthro_emiss* program
9 with the Model for Ozone and Related chemical Tracers (MOZART) species
10 (Supporting Information, Table S3). The *anthro_emiss* program converts the EDGAR-
11 HTAP v2 data into 28 x 28 km² grid by the RACM chemical species (Supporting
12 Information, Table S4). It mapped the MOZART volatile organic compounds (VOC)
13 species into the RACM VOC species (See the detailed equations in Supporting
14 Information, Table S5) (Li et al., 2014; Emmons et al., 2010).

15 The EDGAR-HTAP v3 is extended to much longer time scale than the previous
16 version EDGAR-HTAP (v2). The EDGAR-HTAP v3 covers 2000 to 2018 with a more
17 detailed horizontal resolution (https://edgar.jrc.ec.europa.eu/dataset_htap_v3) (Crippa
18 et al. 2023). While EDGAR-HTAP v2 uses MICS-Asia, only the REAS data are used
19 in China and India in the EDGAR-HTAP v3. It adopts the CAPSS-Konkuk University
20 (CAPSS-KU) data for South Korea and emission data provided by the Japanese
21 government for Japan. We chose the data for 2016, according to the KORUS-AQ
22 campaign period. Because the original EDGAR-HTAP v3 data provide VOC as total
23 NMVOC with the unit of ton/month, we distributed the total NMVOC to MOZART
24 VOC species with the ratio of each VOC species to total NMVOC from EDGAR-HTAP

1 v2 in *anthro_emiss* program. Then, the assigned EDGAR-HTAP v3 data were again
2 converted to the RACM.

3 The KORUS v5 emission data represent 2016 in China and 2015 in other regions.
4 The Comprehensive Regional Emissions Inventory for Atmospheric Transport
5 Experiment (CREATE) v2.3 data from 2015 were used and the ship emissions from
6 CAPSS were added near the coastal region in South Korea (Jang et al., 2020; Woo et
7 al., 2012). The CREATE is originally developed by combining REAS, MEIC, Japan
8 Auto-Oil Program emission inventory (JATOP), and Korean Clear Air Policy Support
9 System (CAPSS). The NMVOC species from KORUS v5 were mapped following the
10 Statewide Air Pollution Research Center (SAPRC-99) mechanism, and we also
11 assigned the SAPRC-99 species to RACM (Carter, 2000) (Supporting information,
12 Table S5-64).

13 Figure 1 shows the spatial distribution of NO, CO, and TOL (toluene + less reactive
14 aromatics defined in RACM, see Table S4) emissions in May for each inventory. The
15 NO_x emissions were assumed to be emitted as NO. The major cities in China and South
16 Korea had relatively high NO, CO, and TOL ~~(toluene and less aromatics defined in~~
17 ~~RACM, see Table S2)~~ emissions, which are ~~major~~ precursors affecting O₃ formation.
18 We define three boxes representing Eastern China, South Korea, and the Seoul
19 metropolitan area (SMA) and calculated the emissions (see Table S23). In South Korea
20 including SMA, EDGAR-HTAP v3 had the largest NO_x emission among the emission
21 inventories. The KORUS v5 has lower NO_x emissions in Eastern China by 46% and
22 39% compared to EDGAR-HTAP v2 and v3, respectively. The CO emission was the
23 lowest in EDGAR-HTAP v2 in South Korea, being 56% (69%) lower than that in
24 KORUS v5 (EDGAR-HTAP v3). KORUS v5 showed the highest CO emissions in SMA

1 though EDGAR-HTAP v3 showed more CO emissions in South Korea. However,
2 KORUS v5 had the smallest CO emissions in China, being 7% (9%) lower than that in
3 EDGAR-HTAP v2 (v3). The TOL emission from KORUS v5 is higher than those from
4 EDGAR-HTAP v2 (EDGAR-HTAP v3) by 176% (98%) in China. The relative
5 difference of TOL between KORUS v5 and EDGAR-HTAP v2 (EDGAR-HTAP v3) is
6 larger in South Korea by 263%. On the other hand, EDGAR-HTAP v3 have the largest
7 total NMVOC emissions over China than EDGAR-HTAP v2 and KORUS v5 by 38 and
8 27 %, respectively. These discrepancies of VOC emissions may lead to a change in the
9 NO_x/VOC-sensitive regime and O₃ production efficiency. The sensitivity of O₃
10 formation to NO_x emission has discrepancies by its regime, which will be further
11 discussed in section 3.2.

12

13 **2.2.2. The model experiments**

14 The model experiments are summarized in Table 1. The simulations using EDGAR-
15 HTAP v2, v3, and KORUS v5 emissions are named as EDV2, EDV3, and KOV5,
16 respectively. In this study, we found consistent underestimation of CO ~~and VOC₂~~,
17 HCHO, TOL, and XYL for all emissions by -40% (\pm 2%) ~~and~~, -25% (\pm 1%) ~~(HCHO)~~,
18 -67% (\pm 21%), -53% (\pm 18%), respectively, compared to DC-8 in South Korea. Here
19 TOL and XYL are lumped species including toluene and xylene, respectively. This is
20 in line with the results reported by Park et al. (2021), who found that almost every
21 model underestimated CO. Underestimation of CO in East Asia is a well-known feature
22 revealed by many studies. For example, Gaubert et al. (2020) mentioned that CAM-
23 Chem underestimates CO during the KORUS-AQ campaign period and presented a CO

1 compensation method utilizing data assimilation with CO observations. Wada et al.
2 (2012) pointed out that EDGAR v4.1 underestimates anthropogenic CO emissions in
3 China by 45% compared to observation-based estimations of CO emissions. Moreover,
4 underestimation of VOC is also found for all anthropogenic emission inventories.
5 Kwon et al. (2021) estimated top-down emissions of anthropogenic VOCs utilizing
6 Geostationary Trace gas and Aerosol Sensor Optimization spectrometer (GeoTASO).
7 They found that top-down VOC emissions were up to 6.9 times higher than bottom-up
8 emissions (KORUS v5).

9 ~~With~~For all emission inventories, O₃ is underestimated at most ground-based
10 observation sites in South Korea. ~~Therefore, t~~To figure out the potential issue that may
11 affectcauses of negative biases of O₃ in South Korea, we conducted ~~threewe~~ additional
12 model simulations using EDGAR-HTAP v3 that shows the lowest bias of O₃
13 concentrations compared to DC-8 ~~(-14.2 ppb)~~ than EDGAR-HTAP v2 ~~(-16.9 ppb)~~ and
14 KORUS v5 ~~(-18.1 ppb)~~ over the SMA; the mean biases are -16.9, -14.2, and -18.1 ppb
15 with EDV2, EDV3, and KOV5, respectively. ~~OneTwo simulations are-is~~ with twice
16 the anthropogenic CO and VOC emissions in China (EDV3_Ch2) and South Korea
17 (EDV3_Ko2), respectively, and the ~~third simulationother simulation~~ uses double CO
18 and VOC emissions in both China and South Korea (EDV3_ChKo2) to investigate
19 possible improvements in the simulated O₃ and CO from these emission changes. To
20 propose the strategies to improve surface O₃ simulations over China and South Korea,
21 we incorporated 4 additional emission scenarios involving the reduction of NO_x and/or
22 VOC emissions over China. Specifically, we considered the cases with a 50% reduction
23 in NO_x emissions only, a 50% reduction in VOC emissions only, a simultaneous 50%

1 [reduction in both NO_x and VOC emissions, and a 75% reduction in NO_x emissions only.](#)

2 [For more details, refer to Section 4 \(Discussion\).](#)

3

4 **2.3. Observations**

5 **2.3.1. Meteorological data**

6 The meteorological field that WRF-Chem reproduced is ~~evaluated~~[validated](#) with the
7 surface synoptic observation (SYNOP) data operated by the World Meteorological
8 Organization (WMO) (<http://www.meteomanz.com>). Surface temperature, relative
9 humidity, and surface wind speed are adopted for model validation. As the SYNOP data
10 are provided every 3 or 6-hourly, we selected model data when the observation data are
11 available. There were 271 sites in China-Taiwan-Hongkong and 48 sites in South Korea.

12

13 **2.3.2. Ground-based observations**

14 The surface observation network used in this study was obtained from Airkorea in South
15 Korea and the China Ministry of Ecology and Environment (MEE) in China. The
16 Airkorea observation network provides 1-hourly measurements of NO₂, SO₂, CO, O₃,
17 PM₁₀, and PM_{2.5} at suburban, background, roadside, city, and port sites
18 (www.airkorea.or.kr). The concentrations of NO₂, CO, and O₃ are measured using the
19 chemiluminescent, non-dispersive infrared, and ultraviolet photometric methods,
20 respectively. [In South Korea, there are indications of positive biases in NO₂ surface
21 observations, potentially resulting in overestimations of 2~308.9%, particularly at
22 suburban sites in spring \(Jung et al., 2017\).](#) The model data with 28 x 28 km² horizontal

1 resolution were linearly interpolated to the 365 sites in South Korea, and we selected
2 NO₂, O₃, and CO for model validation.–

3 The Chinese observations were provided by MEE through the website
4 (beijingair.sinaapp.com). Surface NO₂ over China was measured using a molybdenum
5 converter, which has the potential for positive biases due to other NO₂-related oxidation
6 products (Dunlea et al., 2007). ~~In South Korea, the positive biases exist regarding NO₂~~
7 ~~surface observations, which could to overestimations of 28.9% at suburban sites in~~
8 ~~spring (Jung et al., 2017).~~ CO was measured using infrared absorption (Zhang and Cao.,
9 2015), and there were 1454 stations in China during the campaign period.

10 For validation of NO₂ and HCHO vertical column density, data from the Pandora
11 spectrometer were used, which the model reproduced with emission inventories at the
12 Olympic Park site (37.5232°N, 127.126°E). The HCHO data from Pandora is corrected
13 because of internal off-gasing to avoid positive biases (Spinei et al., 2021). At the same
14 observation site, surface NO₂ was also measured by a KENTEK NO_x analyzer with
15 photolytic method, and surface O₃ was measured using the same instrument. Ground-
16 based HCHO was measured using Aerodyne QCL. We compared the observed diurnal
17 cycle of vertical column and surface concentrations of NO₂ and HCHO with the model
18 simulations utilizing EDV2, EDV3, and KOV5. We also used ground-based VOC data
19 from gas chromatography flame ionization detector (GC-FID) operated by the Seoul
20 Research Institute of Public Health and Environment (SIHE).

21

1 **2.3.3. Aircraft data**

2 The DC-8 research aircraft, operated by NASA, performed multiple flight
3 measurements with a variety of measuring instruments. We utilized 1 minute interval
4 merged data of O₃, NO₂, CO, HCHO, and VOC along the 20 flight paths (Figure 27).

5 The nearest WRF-Chem grid is selected and then temporally and vertically interpolated
6 to the aircraft data using linear interpolation method to fully utilize the observations.

7 Atmospheric NO₂ and O₃ concentrations were measured using a 4-channel
8 chemiluminescence instrument, with an uncertainty of 100 pptv + 30% and 5 ppbv +
9 10%, respectively. CO concentrations were observed using a diode laser spectrometer,
10 with an uncertainty of 2% or 2 ppbv. The Compact Atmospheric Multi-species
11 Spectrometer (CAMS) was used to measure HCHO concentration, with a possible 3%
12 systematic error (Richter et al., 2015). We also utilized data from the Whole Air Sampler
13 (WAS) to analyze VOC species from different emission inventories (Colman et al.,
14 2001). In this study, we focused on DC-8 observations below a height of 2 km to
15 concentrate on planetary boundary layer (PBL) chemistry. The observation height was
16 determined by GPS altitude above ground level.

17

18 **3. Results**

19 **3.1. The model meteorology simulations**

20 The model temperature and relative humidity were compared with surface observations
21 in China and South Korea. The model-simulated temperature had a slight negative mean
22 bias of -0.91 °C (correlation coefficient R = 0.90) in China, with the largest negative
23 bias in southwestern China. In South Korea, the mean bias was -1.71 °C (R = 0.88). The

1 simulated relative humidity showed a negative bias of -20 to -10% in the North China
2 Plain (NCP) area and a positive bias of 10 to 20% in southwestern China. There was a
3 negative bias of relative humidity over the west coastal area and a positive bias of 10 to
4 20% at most observation stations in South Korea. The correlation coefficients between
5 the model relative humidity and observations were 0.85 and 0.76 for China and South
6 Korea, respectively. Overall, the comparisons showed decent model simulations of
7 meteorology. A negative temperature bias could result in a reduction of isoprene
8 emissions, as illustrated in Figure S3 of the Supporting Information, compared to the
9 estimates based on accurately simulated temperature (Figure S3).~~Even if there is~~
10 ~~negative bias of temperature, leading to a 3.3 % bias in actually emitted emissions, the~~
11 ~~averaged impact on emissions in East Asia is negligible by 0.4 % (Supporting~~
12 ~~Information, Figure S3).~~

13 During the KORUS-AQ campaign period, WRF-Chem accurately simulated the
14 daytime PBL height from a laser ceilometer (CL-31, Vaisala Inc., Finland) observed at
15 Yonsei University in Seoul, South Korea (Lee et al., 2019). But, Travis et al. (2022) has
16 indicated the possibility of PBL height underestimations by CTM. Furthermore, due to
17 limitations of the instrument, the ceilometer has potential to inadequately estimate
18 nighttime PBL height. It is primarily attributed to the method based on aerosol gradients
19 (Jordan et al., 2020). Therefore, the interpretation of simulated nighttime concentrations
20 of air pollutants should be approached with caution. More analysis of meteorological
21 fields, including PBL height, can be found in the Supporting Information (Table S75
22 and Figure S42-S53).

23

3.2. Evaluations with routine surface chemical observational data

The study compared simulated concentrations of O₃, NO₂, and CO with data from routine surface observational networks (Table 2 and Figure 32-76). First, the diurnal variations of the model O₃ using different emissions inventories were compared with observations for each subregion (Table 2 and Figure 32). Overall, all emissions inventories successfully reproduced diurnal variations and absolute values of O₃ for most regions, but there were notable discrepancies in several regions.

In the North China Plain (NCP) region, EDV2 led to a negative model O₃ bias (-12 ppb) with R=0.65, while EDV3 and KOV5 simulated O₃ better with reduced biases and increased correlations (R=0.68-0.71). The high NO_x emissions are higher than relative to the VOC emissions in NCP, leading to a low formaldehyde to NO₂ ratio (FNR) (<10.7), suggesting that the NCP area is in a VOC-limited regime with for all emission inventories (Table 3). Due to the elevated reactive VOC emissions in EDV3 and KOV5 compared to EDV2, both EDV3 and KOV5 show improved O₃ simulations. Similarly, EDV2 had a negative O₃ bias (-17 ppb) with R=0.62 in the Yangtze River Delta (YRD) area, but EDV3 and KOV5 much improved the simulations, which was also observed in the Northeastern China (NEC) area. However, the model O₃ concentrations based on the three emission inventories were overestimated in the Sichuan-Chongqing-Guizhou (SCG) and Southeastern China (SEC) area. In SCG and SEC, the WRF-Chem simulated higher biogenic isoprene emissions compared to anthropogenic TOL and XYL emissions by up to a factor of 10, leading to a high FNR (> 1). In Pearl River Delta (PRD), EDV2 showed the lowest bias (-0.3 ppb) compared to EDV3 and KOV5 because EDV3 and KOV5 have elevated anthropogenic VOC emissions as well as enhanced biogenic isoprene emissions under a VOC-limited

1 regime (Table 3). In the suburban area of Northern China (NOC), all emission
2 inventories reasonably simulated hourly O₃ concentrations.

3 Averaged O₃ was well simulated in South Korea (KOR) with low biases (-1 to 0.7
4 ppb), but a negative bias appears over the Seoul metropolitan area (SMA) with all
5 emissions (-5.5 to -3.5 ppb) (Table 2). The WRF-Chem simulations indicated SMA as
6 a highly NO_x-saturated region (FNR < 0.2), resulting in being extremely VOC-sensitive
7 chemistry regime for O₃ production. The underestimated model O₃ levels in this
8 region suggests implies the possibility of deficient insufficient anthropogenic VOC
9 emissions in SMA across for all emission inventories (Table 3). A detailed This will be
10 more analyzed discussion will be provided in section 3.3.

11 The study also analyzed the mean values of ~~daily maximum 8-hour average (MDA8)~~
12 O₃ concentration at each site and their spatial distributions for the entire campaign
13 period (Figure 43). The spatial distributions of the model MDA8 O₃ were not well
14 correlated with those of the observations. But, notable disparities were observed in
15 simulating MDA8 O₃ when the different emissions were used. For the north and eastern
16 part of China including Beijing and Shanghai, large negative biases disappear when
17 using EDV3 and KOV5. KOV5 only shows a significant correlation with the surface
18 MDA8 O₃ observations (including 929 sites) than EDV2 and EDV3 in China (0.43
19 versus 0.01, 0.20). The correlations between the time series of the model MDA8 O₃ and
20 observations varied at each site, with about 40-60% of sites (depending on the emission
21 inventories) showing a correlation coefficient greater than 0.6 (see Supporting
22 Information, Figure S46), and the locations of these sites were scattered. The correlation
23 slightly improved with hourly O₃ concentrations instead of MDA8 O₃, with about 50-
24 60% of sites having a correlation coefficient greater than 0.6 (Supporting Information,

1 Figure S64). For this metric, high correlations occurred in pollution hot spots north of
2 30°N and the South Coast of China, in which the ratio of HCHO to NO₂ (FNR) was
3 much less than 1, suggesting VOC-limited/NO_x-saturated chemical regime (Supporting
4 Information, Figure S75). The model MDA8 O₃ were underestimated for the pollution
5 hot spots with a low HCHO to NO₂ ratio located north of 30°N, suggesting a possibility
6 of model underestimations of anthropogenic VOC emissions causing model MDA8 O₃
7 biases at these sites. In contrast, the simulated MDA8 O₃ was generally overestimated
8 for sites south of 30°N in which HCHO concentrations were high (Supporting
9 Information, Figure S75). Zhang et al. (2020) reported that simulated biogenic isoprene
10 (ISO) from MEGAN was overestimated compared to observation sites under 35°N in
11 China.

12 The EDV2 and EDV3 showed a positive NO₂ bias over the YRD, NCP, and PRD
13 regions, which include large cities in China (Table 2 and Figure 54-65). On the other
14 hand, EDV2 and EDV3 had ~~small~~low negative NO₂ biases in the NEC and NOC regions,
15 ~~during the daytime, which implies underestimation of NO_x emissions in background~~
16 ~~sites (Figure 54). While EDV2 simulates NEC and NOC as NO_x saturated regime,~~
17 ~~EDV3 and KOV5 shows higher FNR indicating transition and VOC saturated regime,~~
18 ~~respectively. As the lower NO_x change the chemical regime from NO_x saturated to~~
19 ~~VOC saturated with KOV5, higher VOC emissions resulted in the lowest O₃ biases in~~
20 ~~NEC and NOC. However, there are still some underestimations of O₃ even though~~
21 ~~EDV3 and KOV5 are used. Chen et al. (2022) reported that soil NO_x could increase O₃~~
22 ~~concentrations in NEC and NOC about 2-10 ppb.~~All models demonstrated reasonable
23 NO₂ model performance in the SCG region, where MDA8 O₃ was overestimated

1 (Figure ~~32~~ and ~~54~~). In the YRD region, there were large positive NO₂ biases with EDV2,
2 EDV3, and KOV5 (ranging from 6.4 to 22.7 ppb). Liu et al. (2021) reported that YRD
3 is in a VOC-limited regime when using EDV2. The findings indicated that a reduction
4 in NO_x emissions led to an increase in O₃ concentrations, while a reduction in VOC
5 emissions resulted in lower O₃ concentrations. The ~~lower bias of~~ reason why O₃ is well
6 simulated in YRD ~~, even though NO₂ is highly overestimated in this region,~~ can be
7 attributed to the combined influence of higher anthropogenic NO_x emissions and VOC
8 originated from both anthropogenic and biogenic sources (Figure ~~S75~~). In contrast,
9 KOV5 underestimated NO₂ in the NCP region, while EDV2 and EDV3 did not, which
10 implies that KOV5 overestimates O₃ in NCP due to the overpredicted NO_x titration
11 effect on O₃. All emissions showed significant discrepancies compared to NO₂
12 observations in the SEC area, with a low correlation coefficient (0.19 to 0.26). EDV3
13 showed the ~~lowest~~ smallest bias of -1.9 ppb (-0.8 ppb) compared to EDV2 and KOV5
14 in South Korea (SMA) showing most reasonable NO_x emissions in this region. The
15 daily averaged NO₂ exhibited spatial distributions similar to MDA8 O₃ and CO (Figure
16 ~~65~~). The slopes of regression between the three model simulations and observations
17 were 1.31, 1.03, and 0.8 for EDV2, EDV3, and KOV5, respectively, in China. The
18 correlation coefficients between the simulated NO₂ utilizing EDV2, EDV3, and KOV5
19 and surface data were around 0.6 in China. EDV2, EDV3, and KOV5 demonstrated
20 good correlations with observations in South Korea (R = 0.69-0.74). Correlation
21 coefficient (R) was the highest with KOV5 in South Korea (R=0.74).

22 Likewise, the diurnal patterns of Ox (= NO₂ + O₃) are well simulated with all
23 emission inventories (Supporting Information, Figure S8). The spatial distribution and
24 diurnal patterns of Ox are similar to O₃ except YRD (Supporting Information, Figure

1 S9). In YRD, the overestimations of Ox with all emission inventories reveals that same
2 issue of NO₂ overestimations in Figure 5. Even though O₃ is well simulated in this
3 region, the negative impact of NO_x titration to O₃ formation is compensated with the
4 overestimated anthropogenic and biogenic VOC emissions as mentioned above.–

5 The simulated CO was averaged at each site and compared with observations
6 during the KORUS-AQ campaign period (Figure ~~76~~). The three model results showed
7 similar spatial distributions to observations, indicating higher CO concentrations in the
8 NCP, YRD, and PRD regions than their surrounding areas. However, all simulations
9 failed to reproduce the abundance of CO, indicating large negative biases throughout
10 the country. The bias was larger in South Korea than in China.

12 **3.3. Evaluations with the airborne and special surface chemical observations** 13 **during KORUS-AQ**

15 **3.3.1. The aircraft observations**

16 Figure ~~27~~ shows the flight paths flown by the DC-8 during the KORUS-AQ campaign
17 period. In Table ~~43~~, we compare the model results for O₃, NO₂, CO, HCHO, TOL, XYL,
18 ETE (Ethene or OL2), and ISO with the corresponding observed values for all flight
19 tracks under 2 km height in South Korea ~~(Table 3)~~. On average, the model
20 underestimated O₃ by 15-18 ppb, with EDV3 exhibiting the lowest O₃ bias (-15.1 ppb)
21 compared to EDV2 and KOV5 (-16.8 and -17.5 ppb, respectively). All emissions
22 showed positive biases for NO₂ (0.64 to 1.72 ppb), ETE (0.08 to 0.14 ppb), and ISO
23 (0.1 to 0.11 ppb). However, the model significantly underestimated CO, HCHO, TOL,
24 and XYL for all three emissions. Given the large spatial variability of air pollutants in
25 South Korea, we also sampled aircraft data from six regions (see Figure ~~27~~) and

1 compared the three model results with the aircraft observations under 2 km height
2 (Figure 8).

3 The flight tracks that surveyed large power plants and factories in the Chungnam
4 region on a daily basis are shown in Figure S106 in the Supporting Information. The
5 largest negative model O₃ bias was observed over the Chungnam region, with a
6 difference of 38-41 ppb. Emission estimation uncertainties can be significant over this
7 region, where there are large point sources such as coal-burning power plants and
8 petrochemical industries. The model NO₂ agreed with the aircraft observations in SMA,
9 but it tends to overestimate the measurements in the other areas. There were substantial
10 model overestimations of NO₂ with EDV3 over the Chungnam and Busan areas, while
11 KOV5 showed the most reasonable model NO₂ simulations. The model CO near the
12 surface was underestimated in the entire domain, resulting in high negative model CO
13 biases relative to the aircraft observations across the six regions (Figure 8). We
14 additionally conducted sensitivity test to investigate the contribution of CO to O₃
15 concentrations in SMA (Supporting information, Figure S11). Doubling CO emissions
16 in China did not significantly change O₃ concentrations at all levels under 2 km. Only
17 1.4 ppb of O₃ concentrations are changed on average during all flight observations.

18 Additionally, we also evaluated the model HCHO, which can be
19 formed by oxidation of other VOCs but also directly emitted by anthropogenic sources,
20 to investigate potential issue uncertainties in anthropogenic VOC emissions. The
21 model HCHO was underestimated by all emission inventories for all subregions, with
22 negative biases being evident in the SMA, Yellow Sea, and Chungnam regions.

23 Other model VOC species, such as TOL, XYL, ETE, and ISO, were also analyzed.
24 These VOC species are classified by their chemical structures and reactivities in the

1 RACM (Stockwell et al., 1997) (Table S42). For example, TOL includes toluene and
2 relatively less reactive aromatics, while XYL includes xylene and more reactive
3 aromatics. The WAS data from DC-8 were lumped into RACM (Supporting
4 Information Table S86, Lu et al., 2013) and were compared with aircraft observations.
5 When the model TOL or XYL was compared with the observed toluene and xylene, the
6 model using KOV5 reasonably reproduced the observed concentrations (light gray bars
7 in Figure 8). However, the model TOL (even using KOV5) underestimated the observed
8 lumped TOL for most of the regions except for Busan (bars including the dark gray part
9 in Figure 8). The model using KOV5 reasonably reproduced the observed xylene or
10 XYL, except for the Chungnam and Busan regions. The observed ethene (or ETE)
11 concentrations were low (< 0.5 ppb), except for the Chungnam region, where the
12 average of measurements was 2.1 ppb. The model ethene concentration was higher than
13 the observations for the SMA, Kyungbuk, and Busan regions, while it had a large
14 negative bias (-1.6 ~ -1.3 ppb) for the Chungnam region. Regarding ~~isoprene (ISO)~~, one
15 of the most important biogenic VOCs, the model values were larger than the
16 observations by a factor of 2.

17 In summary, underestimated CO and aromatic VOCs are the main features, along
18 with underestimated ozone and HCHO. The largest discrepancies occur over the
19 Chungnam region, where large point sources are located on the west coast of South
20 Korea. The detailed statistics over the SMA and Chungnam area can be obtained from
21 the Supporting Information (Table S97-S108).

22 Figure 9 displays the vertical distributions of observed and simulated O₃ and related
23 species over SMA. The shapes of the simulated profile were in agreement with the
24 observations. Particularly, the model accurately reproduced the observed NO₂ profiles

1 though the surface NO₂ is underestimated by -4.2 to -0.8 ppb in SMA (Table 2 and
2 Figure 9b). The underestimation of simulated surface NO₂ is explained by the
3 overestimation of molybdenum converter method; surface concentrations of NO₂ from
4 molybdenum converter is larger than photolytic converter by 13.6% on average and 64%
5 at 4 pm (Figure 10). Although diurnal pattern of surface NO₂ at 12-20 LT is explained
6 by the overestimation of molybdenum converter, there are still some other possible
7 reasons; 1) the emission factor used in this study is ~~from~~ was developed for the Los
8 Angeles Basin, which may need to be adjusted for ~~that might be not adequate to SMA,~~
9 2) the uncertainty of HOx and ROx radicals from other sources can affect the NO₂
10 concentrations.

11 However, the simulated O₃ and HCHO had negative biases of 16.4 ppb and 0.73
12 ppb, respectively, persisting from the surface to 2 km. Additionally, the simulated CO
13 underestimated the observations by 40% throughout the vertical layer. While the model
14 TOL and XYL, utilizing KOV5, agreed well with the observations below 1 km at surface
15 level and had the lowest bias of -0.88 and -0.12 ppb under 2 km, the results using EDV2
16 and EDV3 substantially underestimated the observations throughout the layer
17 (Supporting information, Table S9). On the other hand, the model simulated ETE and
18 ISO overestimated the observations below 1 km over SMA.

19

20 **3.3.2. The ground-based observations**

21 During the KORUS-AQ campaign, Pandora and surface measurements were co-located
22 at the Olympic Park. Figure 10 compares the observed diurnal cycle of Pandora vertical
23 columns and surface concentrations of NO₂ and HCHO with the model simulations.
24 The photolytic converter was used to measure surface NO₂ to minimize positive bias

1 from the molybdenum converter. All emissions reasonably simulated the diurnal
2 patterns of vertical column and surface NO₂ and HCHO concentrations.

3 The surface NO₂ peak appeared at 07 LT in the model and 08 LT in the observations,
4 associated with the increase of traffic and the under-developed convective boundary
5 layer. On the other hand, the Pandora NO₂ column amount increased from 06 LT to 12
6 LT and stayed at that value throughout the afternoon, indicating the increase of NO_x
7 emissions from morning to afternoon. The model-simulated NO₂ columns agreed with
8 those from Pandora in terms of absolute values and diurnal variations. The opposite
9 patterns between surface and column NO₂ were attributed to the change of boundary
10 layer height; NO₂ is concentrated near the surface layer as mixed layer is shallow in the
11 morning and vertically well mixed during the daytime resulting in low surface NO₂
12 concentrations also shown in (Crawford et al., (2020). On the other hand, vertical
13 column NO₂ concentrations show large values in the afternoon due to the consistent
14 emission of NO_x. The simulated and observed HCHO show similar diurnal variations,
15 but a

16 All three emissions inventories underestimated both column and surface HCHO
17 values by up to -8.5×10^{15} molecules·cm⁻² (-46%) at 7 LT and -0.9 ppbv (-26%) at the
18 surface on average. The underestimations of the model HCHO relative to the Pandora
19 and surface observations are similar to findings from comparisons of the model results
20 with the aircraft data (Figure 9). Therefore, the model VOC performance needs to be
21 investigated at the Olympic Park.

22 The diurnal variations of the model O₃, CO, TOL, and XYL were evaluated against
23 the surface observations at the Olympic Park acquired during the KORUS-AQ
24 campaign (Figure 11). The diurnal pattern and hourly averaged mixing ratio of O₃ were

1 well simulated with the three emission inventories with slight model negative biases.
2 The observed CO was 2.7 times higher than the model on average. Considering the
3 diurnal profile of observed TOL and XYL, KOV5 ~~reduced the model~~ exhibited smaller
4 negative biases ~~from~~ than EDV2 and EDV3, but it still showed negative biases. The
5 model TOL and XYL showed peak concentrations at 08 LT, but the observation had a
6 maximum value at 06 LT. The model biases of XYL (-3.7 to -0.6 ppb, -89 to -20%)
7 were much larger than those in TOL at the surface. Our study demonstrates that the
8 improvement of VOC emission/chemistry representations in the model is necessary for
9 better simulations of air quality over SMA and South Korea.

10

11 **3.4. The model performances over South Korea for the Local and Transport Cases**

12 Previous studies have used meteorological conditions to classify synoptic patterns that
13 affect air pollutant concentrations (Park et al. 2021; Peterson et al. 2019). In contrast,
14 we defined the Transport and Local cases by comparing model results that used the
15 EDV3 base emission and the EDV3 zero-out-Chinese emission (see Figure 12). The
16 Local case comprises May 4, May 20, June 2, and June 3 (Supporting Information,
17 Figure S127), while the Transport case includes May 25, May 26, and May 31
18 (Supporting Information, Figure S138). The Local (Transport) case in this study
19 generally aligns with the Stagnant and Blocking (Transport) cases in Peterson et al.
20 (2019); Stagnant and Blocking is the period that large anticyclone is located over South
21 Korea, and Transport case is the period that South Korea is largely affected by long-
22 range transport of air pollutants by westerly wind. The Local case has a Chinese
23 contribution to O₃ of under 11%, whereas the Transport case has a Chinese contribution
24 to O₃ of over 46%. EDV3 performed better in simulating O₃ for the Transport case

1 compared to EDV2 and KOV5, with a bias of only 2.7 ppb in comparison with the DC-
2 8 airborne observations. In contrast, for the Local case, all emissions had a negative
3 bias ranging from 15.5-18.2 ppb. ~~which implies that the insufficient local emissions~~
4 ~~of O₃ precursors in the emission inventories are much important that the Chinese~~
5 ~~emissions.~~ See the Table [S11 and S129](#) in Supporting Information to obtain detailed
6 information of model performances against DC-8 measurements for different cases.
7 Surface concentrations of O₃ at Olympic Park also exhibited enhanced contributions
8 from Chinese anthropogenic emissions for Transport case (Figure [S149](#)). This section
9 focuses on the model simulations using EDV3 and its modified versions, EDV3_Ch2,
10 [EDV3_Ko2](#) -and EDV3_ChKo2 (doubling Chinese and South Korean CO and VOC
11 emissions).

12 Figure 13 illustrates the biases in the model O₃, CO, and HCHO using EDV3 and
13 its variants relative to DC-8 observations over SMA. The plot highlights differences in
14 biases for the Local and Transport cases. The model O₃ biases were negative, and the
15 absolute values of biases were larger in the Local case than in the Transport case (-20%
16 versus -6%). The model CO biases were also negative, and ~~not only~~ the absolute values
17 of biases ~~but also relative differences~~ were larger in the Transport case than in the Local
18 case. ~~despite the higher CO concentrations in Transport case, which implies that the~~
19 ~~background CO emissions are much biased in East Asia (Table S11).~~ The model HCHO
20 biases were negative and similar for the two cases, except for a larger discrepancy
21 between model and observation in the Local case than in the Transport case;
22 ~~representing deficiency of reactive VOC emissions from local sources in SMA.~~

23 Doubling Chinese CO and VOC emissions (EDV3_Ch2) only slightly reduced
24 biases in the Local case, whereas doubling South Korean CO and VOC emissions

1 [\(EDV_Ko2\)](#) reduced biases more compared to the [EDV3_Ch2](#) case. Doubling South
2 [Korean CO and VOC emissions](#), as well as Chinese CO and VOC emissions (EDV3
3 [ChKo2\)](#) ~~led to the best results in O₃ and CO~~, ~~were necessary to substantially reduce the~~
4 ~~model biases~~ for the Local case. For the Transport case, doubling Chinese CO and VOC
5 emissions reduced biases to almost zero for CO and HCHO, but the model O₃ was much
6 overestimated, with 14% positive biases (from an original bias of -6%). [Doubling South](#)
7 [Korean CO and VOC emissions reduced the biases in O₃ and CO a bit, but](#)
8 [overestimated HCHO. The overestimation of O₃ in Transport case in the EDV3_Ch2](#)
9 [and EDV3_ChKo2 cases can be explained by not only excessive ISO but also](#)
10 [overpredicted background O₃ from doubled CO and VOC emissions in China](#)
11 [\(Supporting information, Table S9-S13\). Doubled CO and VOC emissions](#)
12 [overestimated O₃ concentrations over the Yellow Sea, which implies that the enhanced](#)
13 [background O₃ increase can enhance/increase the O₃ level in SMA \(Supporting](#)
14 [Information, Figure S15\) \(Kim et al., 2023\).](#)

15 Further increasing South Korean CO and VOC emissions [in addition to the increase](#)
16 [of Chinese CO and VOC emissions](#) led to overestimations of O₃ (20%) and HCHO
17 (33%). ~~Even though negative bias of HCHO is compensated by doubling CO and VOC~~
18 ~~emissions in China, the additional increase of South Korea CO and VOC emissions~~
19 ~~(EDV3_ChKo2) still simulates low concentrations of TOL and XYL in the model but~~
20 ~~high concentrations of ETE, which implies that overestimations of other reactive VOCs~~
21 ~~in SMA. The VOC speciation map can be another uncertainty that could affect O₃~~
22 ~~simulations in East Asia.~~ These sensitivity tests modifying EDV3 indicate that increases
23 in CO and VOC emissions over South Korea improve the model O₃, CO, and VOC
24 simulations. However, increasing Chinese VOC (and CO) emissions may overestimate

1 the model O₃ for the studied period.

2 3 4. Discussion: strategy for accurate surface O₃ simulations over urban and 4 regional areas in China and South Korea

5 Due to unprecedentedly rich observational data sets acquired during KORUS-AQ, we
6 investigated the status of O₃ simulations and outlined directions for their improvements
7 in SMA and South Korea. In this section, strategies for the enhanced accuracy of surface
8 O₃ simulations over urban and regional areas in China and South Korea are discussed.
9 The discussion is based on the model simulations incorporating various emission
10 scenarios derived from EDV3. In Figures 14 and 15, diverse emission cases are labeled
11 from C1 to C7. Specifically C1, C2, and C3 correspond to EDV3_ChKo2, EDV3_Ch2,
12 and EDV3_Ko2, respectively. Meanwhile, C4, C5, C6, and C7 represent scenarios
13 involving a 50% reduction in Chinese NO_x emissions, a 50% reduction in Chinese VOC
14 emissions, a simultaneous 50% reduction in both Chinese NO_x and VOC emissions,
15 and a 75% reduction of Chinese NO_x emission, respectively, as discussed in Kim et al.
16 (2023). Examining various options involving the increase and decrease of NO_x and
17 VOC emissions from C1 to C7 sheds light on the direction for improving O₃ simulations.

18 Figure 14 illustrates the model O₃ and NO₂ biases (%) in each region for all cases
19 based on EDV3 (Supporting Information, Table S14-S15 for detailed). EDV3
20 demonstrated good performance in simulating O₃ and NO₂ for the NCP, KOR, NEC,
21 and NOC region. The most substantial model O₃ biases were observed in SCG and SEC,
22 with minimal model NO₂ biases. Conversely, the largest model NO₂ biases were found
23 in YRD and PRD, accompanied by modest model O₃ biases. Improvements are needed
24 for model O₃ in SCG, SEC, YRD, and PRD with reasonable NO₂ simulations. For SCG

1 and SEC, the C5 case (50% VOC emission reduction only) exhibited the lowest O₃
2 biases. Doubled Chinese VOC emission case (C1 and C2) in SCG and SEC resulted in
3 increased O₃ biases to ~100%, compared to 66% in the EDV3 case. In this study, the
4 anthropogenic VOC emissions were reduced. Further reductions of biogenic VOC
5 emissions as well as anthropogenic emissions need to be explored in the future. For
6 SCG and SEC, a reduction in NO_x emissions also led to a slight decrease in O₃ biases.
7 FNR values for the two regions are about 1.3, which turned out to be still VOC-limited
8 or in a transitional state. For the YRD and PRD regions, first, NO_x emissions need to
9 be reduced to improve NO₂ biases in the model. The case C6 (50% reductions in both
10 NO_x and VOC emissions) yielded the most favourable O₃ and NO₂ simulations. Solely
11 reducing NO_x emissions (as in case C4) increase O₃ biases by 25-36% relative to EDV3.
12 The FNR values for YRD and PRD are 0.32 and 0.52, respectively, placing them in the
13 VOC-limited regime (FNR < 1). In general, an increase in Chinese VOC emissions (as
14 observed in cases C1 and C2) resulted in elevated surface ozone levels for all regions,
15 including KOR. For NCP, KOR, NEC, and NOC where the model O₃ and NO₂ agree
16 with the observations, reducing VOC proves to be an effective strategy for decreasing
17 surface O₃.

18 In Figure 15, the model O₃ and NO₂ biases (%) in the 12 mega cities in China and
19 South Korea are illustrated for all cases. Refer to Supporting Information Table S16 and
20 S17 for specific values. EDV3 showed effective performance in simulating O₃ and NO₂
21 for cities such as Beijing, Tianjin, Hangzhou, SMA, and Xian. The most substantial
22 model O₃ biases were observed in Chengdu and Chongqing, with minimal model NO₂
23 biases. In contrast, the notable model NO₂ biases were identified in Shanghai, Nanjing,
24 Guangzhou, Shenzhen, and Wuhan, accompanied by modest model O₃ biases. For

1 Chengdu and Chongqing, situated roughly in SCG, the C5 case (50% VOC emission
2 reduction only) results in the lowest O₃ biases with decent NO₂ simulations. For
3 Shanghai, Nanjing, Guangzhou, Shenzhen, and Wuhan, case C6 (50% reductions in
4 both NO_x and VOC emissions) produced the most favorable O₃ and NO₂ simulations.
5 Simply reducing NO_x emissions (as in case C4) increase O₃ biases in these cities.
6 Overall, the increase in Chinese VOC emissions (cases C1 and C2) resulted in elevated
7 surface ozone levels for all cities, including SMA with an increase in ~~biases~~, ~~biases~~,
8 except for Shanghai. Reduction of only VOC emissions (C5) led to the lowest surface
9 O₃ levels for all cities.

12 **5.4. Summary and conclusions**

13 We conducted sensitivity tests using WRF-Chem with three different bottom-up
14 emission inventories (EDGAR-HTAP v2, v3, and KORUS v5) to investigate the
15 impacts of different emissions on the simulation of O₃ and precursors in East Asia. This
16 study is the first to use EDGAR-HTAP v3 with WRF-Chem v4.4 and extends the
17 validation domain to the whole of China during the KORUS-AQ campaign period. We
18 extensively ~~evaluated~~ these emission inventories using both ground and aircraft
19 observations in East Asia.

20 The three emission inventories accurately reproduced the diurnal profiles and
21 absolute values of surface O₃ for most subregions in China, except for the SCG and
22 SEC areas. However, discrepancies were observed in the model performance for the
23 MDA8 O₃ concentrations, with poor correlations observed over regions with high

1 HCHO concentrations (south of 30°N) and relatively low ratios of FNR (north of 30°N).
2 The emission inventories reasonably reproduced the spatial distribution of daily surface
3 NO₂ concentrations. However, we found that CO was considerably underestimated by
4 the emission inventories over both China and South Korea.

5 We evaluated the model simulations against vertical profile measurements of O₃,
6 NO₂, CO, HCHO, TOL, XYL, ETE, and ISO from the DC-8 aircraft, as well as surface
7 observations over South Korea. The simulated vertical shapes of O₃, NO₂, CO, HCHO,
8 TOL, XYL, ETE, and ISO agreed well with the DC-8 measurements in the SMA,
9 although negative biases were observed for O₃, CO, TOL, XYL, and HCHO, with the
10 largest discrepancy between the model results and observations in the Chungnam area.
11 When we compared the simulations with the surface in-situ measurements and
12 PANDORA observations at the Olympic Park in Seoul, the model accurately
13 reproduced the diurnal patterns of surface and vertical columns of NO₂ and HCHO.
14 However, we found that the model underestimated TOL and XYL. This underestimation
15 of TOL and XYL is one of the reasons why the model underestimates O₃ concentrations,
16 as VOCs contribute to NO to NO₂ conversions resulting in O₃ production via
17 photochemistry.

18 We also classified the flight tracks into two categories: Local and Transport cases.
19 We found that the negative bias of O₃ was much larger under the Local case than the
20 Transport case. When the increment of CO and VOC emissions in South Korea is taken
21 into account, the biases of O₃ are significantly reduced, indicating the need for local
22 emission adjustments to decrease O₃ bias in South Korea.

23 [To improve surface O₃ simulations over China and South Korea using EDV3,](#)
24 [lowering VOC emissions are advantageous for SCG and SEC including urban areas](#)

1 [like Chengdu and Chongqing. Meanwhile, for YRD and PRD regions, as well as cities](#)
2 [such as Shanghai, Nanjing, Guangzhou, Shenzhen, and Wuhan, both NO_x and VOC](#)
3 [emissions should be reduced to enhance model performances. Increase in VOC](#)
4 [emissions adversely affected the model's accuracy in simulating O₃ in China, leading](#)
5 [to increased biases.](#)

6 Our study revealed a consistent overestimation of isoprene over SMA. The
7 uncertainty of biogenic VOC emissions from MEGAN can affect the model O₃
8 performance. Therefore, to achieve more accurate simulations of O₃ in East Asia, it is
9 essential to explore precise representations of both anthropogenic and biogenic VOC
10 emissions.

12 **Code and data availability**

13 WRF-Chem source codes are distributed by NCAR
14 (<https://doi:10.5065/D6MK6B4K>). WRF-Chem v4.4 is available in the GitHub (wrf-
15 model, 2022). The exact version of WRF-Chem codes and configuration files are
16 archived at <https://doi.org/10.5281/zenodo.8260026> (Kim et al., 2023). National
17 Centers for Environmental Prediction (NCEP) FNL data can be accessed from Research
18 Data Archive (RDA) (NCEP, 2019). The CAM-Chem data for boundary conditions is
19 also obtained from RDA (ACOM, 2019). The EDGAR-HTAP v2 data can be
20 downloaded in the website (https://edgar.jrc.ec.europa.eu/dataset_htap_v2). The
21 EDGAR-HTAP v3 is archived on Zenodo (Crippa, 2023). The KORUS-AQ data are
22 available in the website (<https://www-air.larc.nasa.gov/cgi-bin/ArcView/korusaq>)
23 (doi:10.5067/Suborbital/KORUSAQ/DATA01). The EDGAR-HTAP v2, v3, and

1 KORUS v5 data including emission processing programs are available at
2 <https://doi.org/10.5281/zenodo.8260026> (Kim et al., 2023).

3

4 **Author contribution**

5 KMK conducted simulations, analysis and wrote the paper. SWK designed this study,
6 secured funding, performed analysis and wrote the paper. SS supported model set-up
7 and contributed to refining the paper. DRB measured VOC data from DC-8. SC
8 acquired ground-based in-situ VOC data at Olympic Park. JHC performed analysis and
9 wrote the paper. LE and GF assisted in setting up the model emissions and discussed
10 about the model performance. AF measured HCHO data from DC-8. JRH measured
11 Pandora data (NO₂, HCHO). JH retrieved PBL height and discussed about the results.
12 JJ acquired NO₂ data at Olympic Park with different methods. AJW acquired NO₂ and
13 O₃ data from DC-8. JHW and QZ provided emissions inventories and related
14 information. All authors reviewed the manuscript.

15

16 **Competing interests**

17 At least one of the (co-)authors is a member of the editorial board of Geoscientific
18 Model Development.

19

20 **Acknowledgements**

21 This work was supported by the National Research Foundation of Korea (NRF) grant
22 funded by the Korea government (MSIT) (No. 2020R1A2C2014131). S.-W. Kim also
23 acknowledges support from NRF-2018R1A5A1024958. All the computing resources
24 are provided by National Center for Meteorological Supercomputer. The National

1 Center for Atmospheric Research (NCAR) is sponsored by the National Science
2 Foundation (NSF) (NNX16AD96G). We would like to express our gratitude to Glen
3 Diskin for generously providing the CO data from the DC-8 aircraft. We also thanks to
4 Andrew Whitehill and Russell Long for providing the HCHO data from Olympic Park.
5 We would also like to thank Meng Li and Brian McDonald for their valuable
6 discussions, which greatly enhanced our understandings.

7

8 **–References**

9 Ackermann, I. J., Hass, H., Memmesheimer, M., Ebel, A., Binkowski, F. S., and
10 Shankar, U.: Modal aerosol dynamics model for Europe: Development and first
11 applications, *Atmos. Environ.*, 32, 2981-2999, [https://doi.org/10.1016/S1352-](https://doi.org/10.1016/S1352-2310(98)00006-5)
12 2310(98)00006-5, 1998.

13 Ahmadov, R., McKeen, S. A., Robinson, A. L., Bahreini, R., Middlebrook, A. M., de
14 Gouw, J. A., Meagher, J., Hsie, E.-Y., Edgerton, E., Shaw, S., and Trainer, M.: A
15 volatility basis set model for summertime secondary organic aerosols over the eastern
16 United States in 2006, *J. Geophys. Res. Atmos.*, 117, D06301,
17 <https://doi.org/10.1029/2011JD016831>, 2012.

18 Anenberg, S. C., Henze, D. K., Tinney, V., Kinney, P. L., Raich, W., Fann, N., Malley,
19 C. S., Roman, H., Lamsal, L., Duncan, B., Martin, R. V., van Donkelaar, A., Brauer,
20 M., Doherty, R., Jonson, J. E., Davila, Y., Sudo, K., and Kuynlenstierna, J. C.I.:
21 Estimates of the global burden of ambient PM_{2.5}, Ozone, and NO₂ on asthma
22 incidence and emergency room visits, *Environ. Health Perspect.*, 126, 107004,
23 doi.org/10.1289/EHP3766, 2018.

24 Atmospheric Chemistry Observations & Modeling/National Center for Atmospheric
25 Research/University Corporation for Atmospheric Research. 2020. CESM2.1 The
26 Community Atmosphere Model with Chemistry (CAM-chem) Outputs as Boundary
27 Conditions. Research Data Archive at the National Center for Atmospheric Research,
28 Computational and Information Systems Laboratory. [https://doi.org/10.5065/CKR4-](https://doi.org/10.5065/CKR4-GP38)
29 GP38. Accessed: 16 April 2019.

30 Buchholz, R. R., Emmons, L. K., Tilmes, S., and The CESM2 Development Team,
31 (2019). CESM2.1/CAM-chem Instantaneous Output for Boundary Conditions.
32 UCAR/NCAR - Atmospheric Chemistry Observations and Modeling Laboratory. Lat:
33 -5 to 45, Lon: 75 to 145, 28 Nov 2022, doi.org/10.5065/NMP7-EP60.

1 Carter, W. P.: Documentation of the SAPRC-99 chemical mechanism for VOC
2 reactivity assessment, Contract, 92, 95–308,
3 <https://intra.engr.ucr.edu/~carter/pubs/s99doc.pdf> (last access: 9 June 2023), 2000.

4 Chen, S.-H. and Sun, W.-Y.: A one-dimensional time dependent cloud model, *J.*
5 *Meteorol. Soc. Japan*, 80, 99-118, <https://doi.org/10.2151/jmsj.80.99>, 2002.

6 [Choi, J., Henze, D. K., Cao, H., Nowlan, C. R., Abad, G. G., Kwon, H.-A., Lee, H.-M.,](#)
7 [Oak, Y. J., Park, R. J., Bates, K. H., Massakkers, J. D., Wisthaler, A., and Weinheimer,](#)
8 [A. J.: An Inversion Framework for Optimizing Non-Methane VOC Emissions Using](#)
9 [Remote Sensing and Airborne Observations in Northeast Asia During the KORUS-](#)
10 [AQ Field Campaign, *J. Geophys. Res. Atmos.*, 127, e2021JD035844,](#)
11 <https://doi.org/10.1029/2021JD035844>, 2022.

12 Colman, J. J., Swanson, A. L., Meinardi, S., Sive, B. C., Blake, D. R., and Rowland, F.
13 S.: Description of the analysis of a wide range of volatile organic compounds in
14 Whole Air Samples collected during PEM-Tropics A and B, *Anal. Chem.*, 73, 3723-
15 3731, <https://doi.org/10.1021/ac010027g>, 2001.

16 Crawford, J. H., Ahn, J.-Y., Al-Saadi, J., Chang, L., Emmons, L. K., Kim, J., Lee, G.,
17 Park, J.-H., Park, R. J., Woo, J. H., Song, C.-K., Hong, J.-H., Hong, Y.-D., Lefter, B.
18 L., Lee, M., Lee, T., Kim, S., Min, K.-E., Yum, S. S., Shin, H. J., Kim, Y.-W., Choi,
19 J.-S., Park, J.S., Szykman, J. J., Long, R. W., Jordan, C. E., Simpson, I. J., Fried, A.,
20 Dibb, J. E., Cho, S., and Kim, Y. P.: The Korea-United States Air Quality (KORUS-
21 AQ) field study, *Elem. Sci. Anth.*, 9, 00163,
22 <https://doi.org/10.1525/elementa.2020.00163>, 2020.

23 Crippa, M., Guizzardi, D., Butler, T., Keating, T., Wu, R., Kaminski, J., Kuenen, J.,
24 Kurokawa, J., Chatani, S., Morikawa, T., Pouliot, G., Racine, J., Moran, M. D.,
25 Klimont, Z., Manseau, P. M., Mashayekhi, R., Henderson, B. H., Smith, S. J.,
26 Suchyta, H., Muntean, M., Solazzo, E., Banja, M., Schaaf, E., Pagani, F., Woo, J.-H.,
27 Kim, J., Monforti-Ferrario, F., Pisoni, E., Zhang, J., Niemi, D., Sassi, M., Ansari, T.,
28 and Foley, K.: The HTAP_v3 emission mosaic: merging regional and global monthly
29 emissions (2000–2018) to support air quality modelling and policies, *Earth Syst. Sci.*
30 *Data*, 15, 2667–2694, <https://doi:10.5194/essd-15-2667-2023>, 2023.

31 Crippa Monica. (2023). HTAP_v3 emission mosaic [edgar_HTAPv3_2016_*]. Zenodo.
32 <https://doi.org/10.5281/zenodo.7516361>

1 Dunlea, E. J., Herndon, S. C., Nelson, D. D., Volkamer, R. M., San Martini, F., Sheehy,
2 P. M., Zahniser, M. S., Shorter, J. H., Wormhoudt, J. C., Lamb, B. K., Allwine, E. J.,
3 Gaffney, J. S., Marley, N. A., Grutter, M., Marquez, C., Blanco, S., Cardenas, B.,
4 Retama, A., Ramos Villegas, C. R., Kolb, C. E., Molina, L. T., and Molina, M. J.:
5 Evaluation of nitrogen dioxide chemiluminescence monitors in a polluted urban
6 environment, *Atmos. Chem. Phys.*, 7, 2691-2704, [https://doi.org/10.5194/acp-7-](https://doi.org/10.5194/acp-7-2691-2007)
7 2691-2007, 2007.

8 Emmons, L. K., Walters, S., Hess, P. G., Lamarque, J.-F., Pfister, G. G., Fillmore, D.,
9 Granier, C., Guenther, A., Kinnison, D., Laepple, T., Orlando, J., Tie, X., Tyndall, G.,
10 Wiedinmyer, C., Baughcum, S. L., and Kloster, S.: Description and evaluation of the
11 Model for Ozone and Related chemical Tracers, version4(MOZART-4), *Geosci.*
12 *Model Dev.*, 3, 43-67, <https://doi.org/10.5194/gmd-3-43-2010>, 2010.

13 Emmons, L. K., Schwantes, R. H., Orlando, J. J., Tyndall, G., Kinnison, D., Lamarque,
14 J.-F., Marsh, D., Mills, M. J., Tilmes, S., Bardeen, C., Buchholz, R. R., Conley, A.,
15 Gettelman, A., Garcia, R., Simpson, I., Blacke, D. R., Meinardi, S., and Pétron, G.:
16 The Chemistry Mechanism in the Community Earth System Model version 2
17 (CESM2), *J. Adv. Model. Earth Syst.*, 12, e2019MS001882,
18 <https://doi.org/10.1029/2019MS001882>, 2020.

19 Franklin, B. A., Brook, R., and Arden Pope III, C.: Air Pollution and Cardiovascular
20 Disease, *Curr. Probl. Cardiol.*, 40, 207-238,
21 <https://doi.org/10.1016/j.cpcardiol.2015.01.003>, 2015.

22 Gaubert, B., Emmons, L. K., Raeder, K., Tilmes, S., Miyazaki, K., Arellano Jr., A. F.,
23 Elguindi, N., Granier, C., Tang, W., Barré, J., Worden, H. M., Buchholz, R. R.,
24 Edwards, D. P. Franke, P., Anderson, J. L., Sauniois, M., Schroeder, J., Woo, J.-H.,
25 Simpson, I. J., Blake, D. R., Meinardi, S., Wennberg, P. O., Crouse, J., Teng, A.,
26 Kim, M., Dickerson, R. R., He, H., Ren X., Pusede, S. E., and Diskin, G. S.:
27 Correcting model biases of CO in East Asia: impact on oxidant distributions during
28 KORUS-AQ, *Atmos. Chem. Phys.*, 20, 14617–14647, [https://doi.org/10.5194/acp-](https://doi.org/10.5194/acp-20-14617-2020)
29 20-14617-2020, 2020.

30 [Goldberg, D. L., Saide, P. E., Lamsal, L. N., de Foy, B., Lu, Z., Woo, J.-H., Kim, Y.,](#)
31 [Kim, J., Gao, M., Carmichael, G., and Streets, D. G.: A top-down assessment using](#)
32 [OMI NO₂ suggests an underestimate in the NO_x emissions inventory in Seoul, South](#)

1 [Korea, during KORUS-AQ, *Atmos. Chem. Phys.*, 19, 1801-1818,](https://doi.org/10.5194/acp-19-1801-2019)
2 [https://doi.org/10.5194/acp-19-1801-2019, 2019.](https://doi.org/10.5194/acp-19-1801-2019)

3 Grell, G. A.: Prognostic evaluation of assumptions used by cumulus parameterizations,
4 *Mon. Weather Rev.*, 121, 764-787, [https://doi.org/10.1175/1520-](https://doi.org/10.1175/1520-0493(1993)121<0764:PEOAUB>2.0.CO;2)
5 [0493\(1993\)121<0764:PEOAUB>2.0.CO;2](https://doi.org/10.1175/1520-0493(1993)121<0764:PEOAUB>2.0.CO;2), 1993.

6 Grell, G. A. and Dévényi, D.: A generalized approach to parameterizing convection
7 combining ensemble and data assimilation techniques, *Geophys. Res. Lett.*, 29, 38-
8 1-38-4, <https://doi.org/10.1029/2002GL015311>, 2002.

9 Grell, G. A., Peckham, S. E., Schmitz, R., McKeen, S. A., Frost, G., Shamarock, W. C.,
10 and Eder, B.: Fully coupled “online” chemistry within the WRF model, *Atmos.*
11 *Environ.*, 39, 6957-6975, <https://doi.org/10.1016/j.atmosenv.2005.04.027>, 2005.

12 Guenther, A., Karl, T., Harley, P., Wiedinmyer, C., Palmer, P. I., and Geron, C.:
13 Estimates of global terrestrial isoprene emissions using MEGAN (Model of
14 Emissions of Gases and Aerosols from Nature), *Atmos. Chem. Phys.*, 6, 3181-3210,
15 <https://doi.org/10.5194/acp-6-3181-2006>, 2006.

16 Hong, S.-Y. and Noh, Y.: A new vertical diffusion package with an explicit treatment of
17 entrainment processes, *Mon. Weather Rev.*, 134, 2318–2341,
18 <https://doi.org/10.1175/MWR3199.1>. 2006.

19 Jang, Y., Lee, Y., Kim, J., Kim, Y., and Woo, J.-H.: Improvement China point source for
20 improving bottom-up emission inventory, *Asia-Pac. J. Atmos. Sci.*, 56, 107-118,
21 <https://doi.org/10.1007/s13143-019-00115-y>, 2020.

22 Janssens-Maenhout, G., Crippa, M., Guizzardi, D., Dentener, F., Muntean, M., Pouliot,
23 G., Keating, T., Zhang, Q., Kurokawa, J., Wankmüller, R., van der Gon, H. D.,
24 Kuenen J. J. P., Kilmont, Z., Frost, G., Darras, S., Koffi, B., and Li, M.: HTAP_v2.2:
25 a mosaic of regional and global emission grid maps for 2008 and 2010 to study
26 hemispheric transport of air pollution, *Atmos. Chem. Phys.*, 15, 11411-11432,
27 <https://doi.org/10.5194/acp-15-11411-2015>, 2015.

28 Jordan, C. E., Crawford, J. H., Beyersdorf, A. J., Eck, T. F., Halliday, H. S., Vault, B.
29 A., Chang, L.-S., Park, J., Park, R., Lee, G., Kim, H., Ahn, J.-Y., Cho, S., Shin, H. J.,
30 Lee, J. H., Jung, J., Kim, D.-S., Lee, M., Lee, T., Whitehill, A., Szykman, J.,
31 Schueneman, M K., Campuzano-Jost, P., Jimenez, J. L., DiGangi, J. P., Diskin, G. S.,
32 Anderson, B. E., Moore, R. H., Ziemba, L. D., Fenn, M. A., Hair, J. W., Kuehan, R.

1 E., Holz, R. E., Chen, G., Travis, K., Shook, M., Peterson, D. A., Lamb, K. D., and
2 Schwarz, J. P.: Investigation of factors controlling PM_{2.5} variability across the South
3 Korean Peninsula during KORUS-AQ, *Elem. Sci. Anth.*, 8,
4 <https://doi.org/10.1525/elementa.424>, 2020.

5 Jung, J., Lee, J., Kim, B., and Oh, S.: Seasonal variations in the NO₂ artifact from
6 chemiluminescence measurements with a molybdenum converter at a suburban site
7 in Korea (downwind of the Asian continental outflow) during 2015-2016, *Atmos.*
8 *Environ.*, 165, 290-300, <https://doi.org/10.1016/j.atmosenv.2017.07.010>, 2017.

9 Kim, K.-M., Kim, S.-W., Choi, M., Kim, M., Kim J., Shina, I., Kim, J., Chung, C.Y.,
10 Yeo, H., Kim, S.-W., Joo, S. J., MckKeen, S. A., and Zhang, L.: Modeling Asian Dust
11 Storms Using WRF-Chem During the DRAGON-Asia Field Campaign in April 2012,
12 *J. Geophys. Res. Atmos.*, 126, e2021JD034793,
13 <https://doi.org/10.1029/2021JD034793>, 2021.

14 Kim, K.-M., Kim, S.-W., Seo, S., Blake, D. R., Cho, S., Crawford, J. H., Emmons, L.,
15 Fried, A., Herman, J. H., Hong, J., Jung, J., Pfister, G., Weinheimer, A. J., Woo, J.-
16 H., and Zhang, Q.: WRF-Chem configurations and input data sets for sensitivity tests
17 of emission inventories, Zenodo [Data set], <https://doi.org/10.5281/zenodo.8260026>,
18 2023.

19 Kim, S.-W., McDonald, B. C., Baidar, S., Brown, S. S., Dube, B., Ferrare, R. A., Frost,
20 G. J., Harley, R. A., Holloway, J. S., Lee, H.-J., McKeen, S. A., Neuman, J. A., Bowak,
21 J. B., Oetjen, H., Ortega, I., Pollack, I. B., Roberts, J. M., Ryerson, T. B., Scarino, A.
22 J., Senff, C. J., Thalman, R., Trainer, M., Volkamer, R., Wagner, N., Washenfelder, R.
23 A., Waxman, E., and Young, C. J.: Modeling the weekly cycle of NO_x and CO
24 emissions and their impacts on O₃ in the Los Angeles-South Coast Air Basin during
25 the CalNex 2010 field campaign, *J. Geophys. Res. Atmos.*, 121, 1340-1360,
26 <https://doi.org/10.1002/2015JD024292>, 2016.

27 [Kim, S.-W., Kim, K.-M., Jeong, Y., Seo, S., Park, Y., and Kim J.: Changed in surface](#)
28 [ozone in South Korea on diurnal to decadal timescales for the period of 2001-2021,](#)
29 [*Atmos. Chem. Phys.*, 23, 12867-12886, <https://doi.org/10.5194/acp-23-12867-2023>,](#)
30 [2023.](#)

31 Kwon, H.-A., Park, R. J., Oak, Y. J., Nowlan, C. R., Janz, S. J., Kowalewski, M. G.,
32 Fried, A., Walega, J., Bates, K. H., Choi, J., Blake, D. R., Wisthaler, A., and Woo, J.-

1 H.: Top-down estimates of anthropogenic VOC emissions in South Korea using
2 formaldehyde vertical column densities from aircraft during the KORUS-AQ
3 campaign, *Elem. Sci. Anth.*, 9, 00109, <https://doi.org/10.1525/elementa.2021.00109>,
4 2021.

5 Kurokawa, J. and Ohara, T.: Long-term historical trends in air pollutant emissions in
6 Asia: Regional Emission inventory in ASia (REAS) version 3, *Atmos. Chem. Phys.*,
7 20, 12761-12793, <https://doi.org/10.5194/acp-20-12761-2020>, 2020.

8 Lee, B.-J., Kim, B., and Lee, K.: Air pollution exposure and cardiovascular disease,
9 *Toxicol. Res.*, 30, 71-75, <https://doi.org/10.5487/TR.2014.30.2.071>, 2014.

10 Lee, J. H., Hong, J.-W., Lee, K. M., Hong, J., Velasco, E., Lim, Y., Lee, J., Nam, K.,
11 and Park, J.: Ceilometer monitoring of boundary layer height in Seoul and its
12 application to evaluate the dilution effect on air pollution, *Boundary Layer Meteorol.*,
13 171, 435-455, <https://doi.org/10.1007/s10546-019-00452-5>, 2019.

14 Li, M., Zhang, Q., Streets, D. G., He, K. B., Cheng, Y. F., Emmons, L. K., Huo, H.,
15 Kang, S. C., Lu, Z., Shao, M., Su, H., Yu, X., and Zhang, Y.: Mapping Asian
16 anthropogenic emissions of non-methane volatile organic compounds to multiple
17 chemical mechanisms, *Atmos. Chem. Phys.*, 14, 5617-5638,
18 <https://doi.org/10.5194/acp-14-5617-2014>, 2014.

19 Li, Q., Zhang, L., Wang, T., Tham, Y. J., Ahmadov, R., Xue, L., Zhang, Q., and Zheng,
20 J.: Impacts of heterogeneous uptake of dinitrogen pentoxide and chlorine activation
21 on ozone and reactive nitrogen partitioning: improvement and application of the
22 WRF-Chem model in southern China, *Atmos. Chem. Phys.*, 16, 14875–14890,
23 <https://doi.org/10.5194/acp-16-14875-2016>, 2016.

24 Liu, Z., Doherty, R. M., Wild, O., Hollaway, M., and O'Connor, F. M.: Contrasting
25 chemical environments in summertime for atmospheric ozone across major Chinese
26 industrial regions: the effectiveness of emission control strategies, *Atmos. Chem.*
27 *Phys.*, 21, 10689-10706, <https://doi.org/10.5194/acp-21-10689-2021>, 2021.

28 Lu, K. D., Hofzumahaus, A., Holland, F., Bohn, B., Brauers, T., Fuchs, H., Hu, M.,
29 Häsel, R., Kita, K., Kondo, Y., Li, X., Lou, S. R., Oebel, A., Shao, M., Zheng, J.
30 M., Wahner, A., Zhu, T., Zhang, T. H., and Rohrer, F.: Missing OH source in a
31 suburban environment near Beijing: observed and modelled OH and HO₂

1 concentrations in summer 2006, *Atmos. Chem. Phys.*, 13, 1057-1080,
2 doi.org/10.5194/acp-13-1057-2013, 2013.

3 Madronich, S.: Photodissociation in the Atmosphere, 1, actinic flux and the effects of
4 ground reflections and clouds, *J. Geophys. Res. Atmos.*, 92, 9740–9752.
5 <https://doi.org/10.1029/JD092iD08p09740>, 1987.

6 Manning, W. J. and von Tiedemann, A. Climate change: Potential effects of increased
7 atmospheric carbon dioxide (CO₂), ozone (O₃), and ultraviolet-B (UV-B) radiation
8 on plant diseases, *Environ. Pollut.*, 88, 219-245, [https://doi.org/10.1016/0269-](https://doi.org/10.1016/0269-7491(95)91446-R)
9 [7491\(95\)91446-R](https://doi.org/10.1016/0269-7491(95)91446-R), 1995.

10 [Miyazaki, K., Sekiya, T., Fu, D., Bowman, K. W., Kulawik, S. S., Sudo, K., Walker, T.,](#)
11 [Kanaya, Y., Takigawa, M., Ogochi, K., Eskes, H., Boersma, K. F., Thompson, A. M.,](#)
12 [Gaubert, B., Barre, J., and Emmons, L. K.: Balance of Emission and Dynamical](#)
13 [Controls on Ozone During the Korea-United States Air Quality Campaign From](#)
14 [Multiconstituent Satellite Data Assimilation, *J. Geophys. Res. Atmos.*, 124, 387-413,](#)
15 <https://doi.org/10.1029/2018JD028912->, 2019.

16 National Centers for Environmental Prediction/National Weather Service/NOAA/U.S.
17 Department of Commerce. 2000, updated daily. NCEP FNL Operational Model
18 Global Tropospheric Analyses, continuing from July 1999. Research Data Archive at
19 the National Center for Atmospheric Research, Computational and Information
20 Systems Laboratory. <https://doi.org/10.5065/D6M043C6>. Accessed: 25 March 2019.

21 Park, R. J., Oak, Y. J., Emmons, L. K., Kim, C.-H., Pfister, G. G., Carmichael, G. R.,
22 Saide, P. E., Cho, S.-Y., Kim, S., Woo, J.-H., Crawford, J. H., Gaubert, B., Lee, H.-
23 J., Park, S.-Y., Jo, Y.-J., Gao, M., Tang, B., Stanier, C. O., Shin, S. S., Park, H. Y.,
24 Bae, C., and Kim, E.: Multi-model intercomparisons of air quality simulations for
25 the KORUS-AQ campaign, *Elem. Sci. Anth.*, 9, 00139,
26 <https://doi.org/10.1525/elementa.2021.00139>, 2021.

27 Peterson, D. A., Hyer, E. J., Han, S.-O., Crawford, J. H., Park, R. J., Holz, R., Kuehn,
28 R. E., Eloranta, E., Knote, C., Jordan, C. E., and Lefer, B. L.: Meteorology
29 influencing springtime air quality, pollution transport, and visibility in Korea, *Elem.*
30 *Sci. Anth.*, 7, 57, <https://doi.org/10.1525/elementa.395>, 2019.

- 1 Richter, D., Weibring, P., Walega, J. G., Fried, A., Supler, S. M., and Taubman, M. S.:
2 Compact highly sensitive multi-species airborne mid-IR spectrometer, *Appl. Phys. B*,
3 119, 119-131, <https://doi.org/10.1007/s00340-015-6038-8>, 2015.
- 4 Rosenzweig, C., Karoly, D., Vicarelli, M., Neofotis, P., Wu, Q., Casassa, G., Menzel,
5 A., Root, T. L., Estrella, N., Seguin, B., Tryjanowski, P., Liu, C., Rawlins, S., and
6 Imeson, A.: Attributing physical and biological impacts to anthropogenic climate
7 change, *Nature*, 453, 353-357, <https://doi.org/10.1038/nature06937>, 2008.
- 8 Saikawa, E., Kim, H., Zhong, M., Avramov, A., Zhao, Y., Janssens-Maenhout, G.,
9 Kurokawa, J.-I., Klimont, Z., Wagner, F., Naik, V., Horowitz, L. W., and Zhang, Q.:
10 Comparison of emissions inventories of anthropogenic air pollutants and greenhouse
11 gases in China, *Atmos. Chem. Phys.*, 17, 6393-6421, <https://doi.org/10.5194/acp-17-6393-2017>, 2017.
- 13 Sharma, A., Ojha, N., Pozzer, A., Mar, K. A., Beig, G., Lelieveld, J., and Gunthe, S. S.:
14 WRF-Chem simulated surface ozone over south Asia during the pre-monsoon:
15 effects of emission inventories and chemical mechanisms, *Atmos. Chem. Phys.*, 17,
16 14393-14414, <https://doi.org/10.5194/acp-17-14393-2017>, 2017.
- 17 Sicard, P., Crippa, P., De Marco, A., Castruccio, S., Giani, P., Cuesta, J., Paoletti, E.,
18 Feng, Z., and Anav, A.: High spatial resolution WRF-Chem model over Asia: Physics
19 and chemistry evaluation, *Atmos. Environ.*, 244, 118004,
20 <https://doi.org/10.1016/j.atmosenv.2020.118004>, 2021.
- 21 [Souri, A. H., Nowlan, C. R., Abad, G. G., Zhu, L., Blake, D. R., Fried, A., Weinheimer,](#)
22 [A. J., Wisthaler, A., Woo, J.-H., Zhang, Q., Chan Miller, C. E., Liu, X., and Chance,](#)
23 [K.: An inversion of NO_x and non-methane volatile organic compound \(NMVOC\)](#)
24 [emissions using satellite observations during the KORUS-AQ campaign and](#)
25 [implications for surface ozone over East Asia, *Atmos. Chem. Phys.*, 20, 9837-9854,](#)
26 <https://doi.org/10.5194/acp-20-9837-2020>, 2020.
- 27 Spinei, E., Tiefengraber, M., Müller, M., Gebetsberger, M., Cede, A., Valin, L.,
28 Szykman, J., Whitehill, A., Kotsaki, A., Santos, F., Abbuhasan, N., Zhao, X., Fioletov,
29 V., Lee, S. C., and Swap, R.: Effect of polyoxymethylene (POM-H Delrin) off-
30 gassing within the Pandora head sensor on direct-sun and multi-axis formaldehyde
31 column measurements in 2016–2019, *Atmos. Meas. Tech.*, 14, 647-663,
32 <https://doi.org/10.5194/amt-14-647-2021>, 2021.

- 1 Stockwell, W. R., Kirchner, F., and Kuhn, M.: A new mechanism for regional
2 atmospheric chemistry modeling, *J. Geophys. Res. Atmos.*, 102, 25847-25879,
3 <https://doi.org/10.1029/97JD00849>, 1997.
- 4 [Tang, W., Emmons, L. K., Arellano Jr, A. F., Gaubert, B., Knote, C., Tilmes, S.,](#)
5 [Buchholz, R. R., Pfister, G. G., Diskin, G. S., Blake, D. R., Blake, N. J., Meinardi,](#)
6 [S., DiGangi, J. P., Choi, Y., Woo, J.-H., He, C., Schroeder, J. R., Suh, I., Lee, H.-J.,](#)
7 [Kanaya, Y., Jung, J., Lee, Y., and Kim, D.: Source Contributions to Carbon Monoxide](#)
8 [Concentrations During KORUS-AQ Based on CAM-chem Model Applications, *J.*](#)
9 [Geophys. Res. Atmos., 124, 2796-2822, <https://doi.org/10.1029/2018JD029151>, 2019.](#)
- 10 Tewari, M., F. Chen, W. Wang, J. Dudhia, M. A. LeMone, K. Mitchell, M. Ek, G. Gayno,
11 J. Wegiel, and Cuenca, R. H.: Implementation and verification of the unified NOAA
12 land surface model in the WRF model, *20th conference on weather analysis and*
13 *forecasting/16th conference on numerical weather prediction*, pp. 11–15, 2004.
- 14 Travis, K. R., Crawford, J. H., Chen, G., Jordan, C. E., Nault, B. A., Kim, H., Jimenez,
15 J. L., Campuzano-Jost, P., Dibb, J. E., Woo, J.-H., Kim, Y., Zhai, S., Wang, X.,
16 McDuffie, E. E., Luo, G., Yu, F., Kim, S., Simpson, I. J., Blake, D. R., Chang, L.,
17 and Kim, M. J.: Limitations in representation of physical processes prevent
18 successful simulation of PM_{2.5} during KORUS-AQ, *Atmos. Chem. Phys.*, 22, 7933–
19 7958, <https://doi.org/10.5194/acp-22-7933-2022>, 2022.
- 20 Wada, A., Matsueda, H., Murayama, S., Taguchi, S., Kamada, A., Nosaka, M., Tsuboi,
21 K., and Sawa, Y.: Evaluation of anthropogenic emissions of carbon monoxide in East
22 Asia derived from the observations of atmospheric radon-222 over the western North
23 Pacific, *Atmos. Chem. Phys.*, 12, 12119–12132, [https://doi.org/10.5194/acp-12-](https://doi.org/10.5194/acp-12-12119-2012)
24 [12119-2012](https://doi.org/10.5194/acp-12-12119-2012), 2012.
- 25 [Wiedinmyer, C., and Emmons, L.: Fire Inventory from NCAR version 2 Fire Emission,](#)
26 [Research Data Archive at the National Center for Atmospheric Research,](#)
27 [Computational and Information Systems Laboratory, \[https://doi.org/10.5065/XNPA-\]\(https://doi.org/10.5065/XNPA-AF09\)](#)
28 [AF09, 2022. last access: 17 Oct 2023.](#)
- 29 Wild, O., Prather, M. J., and Akimoto, H.: Indirect long-term global radiative cooling
30 from NO_x Emissions, *Geophys. Res. Lett.*, 28, 1719-1722,
31 <https://doi.org/10.1029/2000GL012573>, 2001.

1 Woo, J.-H., Choi, K.-C., Kim, H. K., Baek, B. H., Jang, M., Eum, J.-H., Song, C. H.,
2 Ma, Y.-I., Sunwoo, Y., Chang, L.-S., and Yoo, S. H.: Development of an
3 anthropogenic emissions processing system for Asia using SMOKE, *Atmos. Environ.*,
4 58, 5-13, <https://doi.org/10.1016/j.atmosenv.2011.10.042>, 2012.

5 wrf-model: WRF, Github [code], <https://github.com/wrf-model/WRF/releases/tag/v4.4>,
6 last access: 18 May 2022.

7 Zhang, Y.-L. and Cao, F.: Fine particulate matter (PM_{2.5}) in China at a city level, *Sci.*
8 *Rep.*, 5, 14884, <https://doi.org/10.1038/srep14884>, 2015.

9 Zhang, Y., Zhang, R., Yu, J., Zhang, Z., Yang, W., Zhang, H., Lyu, S., Wang, Y., Dai,
10 W., Wang, Y., and Wang, X.: Isoprene Mixing Ratios Measured at Twenty Sites in
11 China During 2012–2014: Comparison With Model Simulation, *J. Geophys. Res.*
12 *Atmos.*, 125, e2020JD033523, <https://doi.org/10.1029/2020JD033523>, 2020.

13 Zheng, B., Tong, D., Li, M., Liu, F., Hong, C., Geng, G., Li, H., Li, X., Peng, L., Qi, J.,
14 Yan, L., Zhang, Y., Zhao, H., Zheng, Y., He, K., and Zhang, Q.: Trends in China's
15 anthropogenic emissions since 2010 as the consequence of clean air actions, *Atmos.*
16 *Chem. Phys.*, 18, 14095–14111, <https://doi.org/10.5194/acp-18-14095-2018>, 2018.

17 Zhong, M., Saikawa, E., Liu, Y., Naik, V., Horowitz, L. W., Takigawa, M., Zhao, Y.,
18 Lin, N.-H., and Stone, E. A.: Air quality modeling with WRF-Chem v3.5 in East Asia:
19 sensitivity to emissions and evaluation of simulated air quality, *Geosci. Model Dev.*,
20 9, 1201–1218, <https://doi.org/10.5194/gmd-9-1201-2016>, 2016.

1 **Table List**

2

3 Table 1. The model experiments with different emissions.

4

5 Table 2. Comparison of the ground-based hourly O₃, NO₂, and CO observations with
6 the simulations utilizing EDGAR-HTAP v2 (EDV2) and v3 (EDV3) and KORUS v5
7 (KOV5) in each regional box (unit = ppb). N is the number of samples. R is correlation
8 coefficient.

9

10 Table 3. Comparison of total NO_x, TOL, XYL, biogenic isoprene emissions, and
11 formaldehyde to NO₂ ratio (FNR) for different emission data sets in each regional box.
12 The MEGAN biogenic isoprene emissions are equally applied to all simulations using
13 different emission data. (unit = mol/s for emissions)

14

15 Table 43. Comparison of aircraft-based 1-minute-interval O₃, NO₂, CO, HCHO, TOL,
16 XYL, ETE, and ISO observations with EDV2, EDV3, and KOV5 for all flight cases
17 under 2 km height (unit = ppb). N is the number of samples. R is correlation coefficient.

1 **Figure List**

2

3 Figure 1. The averaged spatial distribution map of the NO, CO, and TOL (toluene + less
4 reactive aromatics) emissions from EDGAR-HTAP v2, v3, and KORUS v5 in May. The
5 boxes represent Northern China (NOC, 38-42°N/106-110°E), Sichuan-Chongqing-
6 Guizhou (SCG, 27-33°N/103-109°E), Pearl River Delta (PRD, 21.5-24°N/112-115.5°E),
7 Southeastern China (SEC, 24-28°N/116-120°E), Yangtze River Delta (YRD, 30-
8 33°N/119-122°E), South Korea (KOR, 34.5-38°N/126-130°E), North China Plain (NCP,
9 34-41°N/113-119°E), and Northeastern China (NEC, 43-47°N/124-130°E). NOC, NEC,
10 and SEC are denoted by blue boxes (non-urban). NCP, SCG, PRD, YRD, and KOR are
11 denoted by red boxes (urban).

12

13 Figure 72. The DC-8 flight paths during the KORUS-AQ campaign period (black) and
14 6 regional boxes (1: Seoul Metropolitan Area (SMA); 2: Yellow Sea; 3: Chungnam; 4:
15 Kyungbuk; 5: Gwangju; 6: Busan) (red).

16

17 Figure 23. Averaged O₃ concentrations from ground-based observations and model
18 simulations over the areas that distinguish urban (red box) and non-urban (green box)
19 region (central plot). Box-averaged diurnal cycle (solid lines) of O₃ and 1/4 of standard
20 deviations (filled area) from observations (black), EDV2 (greensky blue), EDV3 (blue),
21 and KOV5 (red) by local time are shown. The results are shown for ~~Northern China~~
22 ~~(NOC, 38-42°N/106-110°E), Sichuan-Chongqing-Guizhou (SCG, 27-33°N/103-109°E),~~
23 ~~Pearl River Delta (PRD, 21.5-24°N/112-115.5°E), Southeastern China (SEC, 24-~~
24 ~~28°N/116-120°E), Yangtze River Delta (YRD, 30-33°N/119-122°E), South Korea~~
25 ~~(KOR, 34.5-38°N/126-130°E), North China Plain (NCP, 34-41°N/113-119°E), and~~
26 ~~Northeastern China (NEC, 43-47°N/124-130°E).~~

27

28 Figure 43. Comparison of (a) the campaign averaged ground-based maximum daily
29 average of 8-hour O₃ (MDA8 O₃) (unit: ppb) observations and WRF-Chem simulations
30 with (d) EDGAR-HTAP v2 (EDV2), (e) v3 (EDV3), (f) KORUS v5 (KOV5) and (g, h,
31 i) the differences between the observations and model results. The sub-regions are
32 presented with red (urban) and green (non-urban) boxes. The scatter plots comparing
33 averaged observations and the three-emission-based WRF-Chem simulations (greensky
34 blue; EDV2, blue; EDV3, red; KOV5) are shown in (b) and (c) for Eastern China and
35 South Korea, respectively. (a, d-e) Color-filled circles in (a), (d), (e), and (f) represent
36 the averaged MDA8 O₃ for the whole campaign period (1st May to 10th June).

37

38 Figure 45. The same as Figure 23 except NO₂.

39

1 Figure 56. The same as Figure 34 except daily NO₂ (unit: ppb).

2

3 Figure 67. The same as Figure 34 except daily CO (unit: ppm).

4

5 ~~Figure 7. The DC-8 flight paths during the KORUS AQ campaign period (black) and 6~~
6 ~~regional boxes (1: Seoul Metropolitan Area (SMA); 2: Yellow Sea; 3: Chungnam; 4:~~
7 ~~Kyungbuk; 5: Gwangju; 6: Busan) (red).~~

8

9 Figure 8. The mean (bars) and 1/4 of standard deviations (whiskers) of (a) O₃, (b) NO₂,
10 (c) CO, (d) HCHO, (e) TOL, (f) XYL, (g) ethene (ETE), and (h) isoprene (ISO) (unit =
11 ppb) from DC-8 (dark grey), EDV2 (greensky blue), EDV3 (blue), and KOV5 (red) for
12 each box are shown, respectively. TOL and XYL are calculated based on Table S68
13 (Supporting Information). The contribution of toluene to TOL and m/p-Xylene + o-
14 Xylene to XYL is represented with light grey bars (e, f). The sampling numbers are
15 represented with magenta color above the plots.

16

17 Figure 9. Vertically averaged (a) O₃, (b) NO₂, (c) CO, (d) HCHO, (e) TOL, (f) XYL, (g)
18 ETE, and (h) ISO from DC-8 (black), EDV2 (greensky blue), EDV3 (blue), and KOV5
19 (red) in SMA under 2 km height above ground level. The 1/2 of standard deviations are
20 represented with black whiskers in each 200m layer. The sample number is presented
21 with magenta color on the right side of the plots.

22

23 Figure 10. The diurnal cycles of vertical columns and surface concentrations of (a) NO₂
24 and (b) HCHO from Pandora spectrometer (column), and ground-based instruments
25 (TEI 42i NO_x analyzer and Aerodyne QCL) at the Olympic Park site (37.5232°N,
26 127.126°E). EDV2 (greensky blue), EDV3 (blue), and KOV5 (red) are compared with
27 observations. The WRF-Chem vertical column concentrations are produced by
28 summing all vertical layers.

29

30 Figure 11. Diurnal cycles of surface (a) O₃, (b) CO, (c) TOL, and (d) XYL at the
31 Olympic Park site. EDV2 (greensky blue), EDV3 (blue), and KOV5 (red) are compared
32 with the observations. 1/4 of standard deviations are represented with grey shades. The
33 average period is from the 11th May to the 10th June.

34

35 Figure 12. Averaged O₃ (bars) and 1/4 of standard deviations (whiskers) (unit: ppbv)
36 for the 20 DC8 flights (under 2 km height). The observations (grey) are compared with
37 the model results utilizing EDV2 (greensky blue), EDV3 (blue), and KOV5 (red).

1 White hatch-filled bars over blue bars are the contribution of Chinese emissions to O₃
2 concentrations obtained from the default and sensitivity model runs with/without
3 Chinese anthropogenic emissions. The Local (5/4,20 and 6/2,3) and Transport
4 (5/25,26,31) cases are shaded with light blue and orange, respectively.

5

6 Figure 13. The biases in (a) the model O₃, (b) CO, and (c) HCHO concentrations (bars)
7 relative to the DC-8 observations under 2 km height over SMA (dark gray: EDV3, red:
8 EDV3 Ch2, blue: EDV3 ChKo2): (left panel) Local and (right panel) Transport case.
9 Fractional differences (%) are shown in the white boxes.

10

11 Figure 14. Comparison of relative biases ((Model-Observation)/Observation, unit=%)
12 of daily O₃ and NO₂ at surface observation sites during the KORUS-AQ campaign
13 period from sensitivity simulation (C1-7) with EDV3 in each region (NCP, SCG, YRD,
14 PRD, KOR, NEC, NOC, and SEC). C1; EDGAR-HTAP v3 with double CO and VOC
15 emission in China and South Korea, C2; EDGAR-HTAP v3 with double CO and VOC
16 emission in China, C3; EDGAR-HTAP v3 with double CO and VOC emission in South
17 Korea, C4; EDGAR-HTAP v3 with 50% NO_x reduction in China, C5; EDGAR-HTAP
18 v3 with 50% VOC reduction in China, C6; EDGAR-HTAP v3 with 50% NO_x and VOC
19 reduction in China, C7; EDGAR-HTAP v3 with 75% NO_x reduction in China.

20

21 Figure 15. Same as Figure 14 except that the region is changed to cities; Beijing (39.4-
22 41.1N, 115.4-117.5E), Tianjin (38.55-40.25N, 116.7-118.1E), Chengdu (30.05-31.5N,
23 103-105E), Chongqing (28.15-32.25N, 105.3-110.2E), Shanghai (30.7-31.5N, 120.85-
24 122E), Hangzhou (29.2-30.6N, 118.3-120.9E), Nanjing (31.2-32.65N, 118.35-119.25E),
25 Guangzhou (22.55-24N, 112.9-114.05E), Shenzhen (22.4-22.9N, 113.7-114.65E),
26 SMA (37.2-37.8N, 126.5-127.3E), Wuhan (29.95-31.4N, 113.65-115.1E), and Xian
27 (33.65-34.75N, 107.65-109.9E).

1 **Table 1.** The model experiments with different emissions

Experiments	Emissions
EDV2	EDGAR-HTAP-v2
EDV3	EDGAR-HTAP-v3
KOV5	KORUS-v5
EDV3_Ch2	EDGAR-HTAP-v3 with double CO, VOC emission in China
EDV3_ChKo2	EDGAR-HTAP-v3 with double CO, VOC emission in China & South Korea

2

1 **Table 1.** [The model experiments with different emissions.](#)

<u>Esxperiments</u>	<u>Emissions</u>
<u>EDV2</u>	<u>EDGAR-HTAP v2</u>
<u>EDV3</u>	<u>EDGAR-HTAP v3</u>
<u>KOV5</u>	<u>KORUS v5</u>
<u>EDV3 Ch2</u>	<u>EDGAR-HTAP v3 with double CO, VOC emission in China</u>
<u>EDV3 Ko2</u>	<u>EDGAR-HTAP v3 with double CO, VOC emission in South Korea</u>
<u>EDV3 ChKo2</u>	<u>EDGAR-HTAP v3 with double CO, VOC emission in China & South Korea</u>

2

3

1 **Table 2.** Comparison of the ground-based hourly O₃, NO₂, and CO observations with
2 the simulations utilizing EDGAR-HTAP v2 (EDV2) and v3 (EDV3) and KORUS v5
3 (KOV5) in each regional box (unit = ppb). N is the number of samples. R is correlation
4 coefficient.

Region		¹⁾ NCP	^{1),a)} SCG	¹⁾ YRD	¹⁾ PRD	^{1),b)} KOR (SMA)	^{2),c)} NEC	^{2),d)} NOC	^{2),e)} SEC		
N		190	104	93	68	358 (125)	45	28	43		
O ₃	OBS	Mean	44.5	34.6	38.2	27.9	41.5 (36.6)	40.9	44.3	26.1	
		Mean	32.2	53.5	21.6	27.6	40.5 (31.1)	28.6	39.4	40.8	
	EDV2	Bias	-12.3	18.9	-16.6	-0.3	-1.0 (-5.5)	-12.3	-4.9	14.7	
		R	0.65	0.53	0.62	0.61	0.59 (0.60)	0.48	0.63	0.52	
		Mean	43.4	57.5	35.7	34.7	41.0 (32.6)	35.2	43.7	45.5	
	EDV3	Bias	-1.1	23.0	-2.5	6.8	-0.5 (-4.0)	-5.7	-0.6	19.4	
		R	0.68	0.55	0.66	0.65	0.56 (0.57)	0.63	0.67	0.55	
		Mean	49.0	55.3	41.1	35.7	42.2 (33.1)	37.1	43.8	42.4	
	KOV5	Bias	4.5	20.7	2.8	7.8	0.7 (-3.5)	-3.8	-0.5	16.3	
		R	0.71	0.53	0.65	0.70	0.62 (0.64)	0.62	0.67	0.54	
	NO ₂	OBS	Mean	17.5	13.8	17.1	12.9	23.2 (32.5)	13.5	11.9	9.6
			Mean	25.8	12.7	39.8	22.0	18.8 (29.6)	13.7	12.9	11.0
EDV2		Bias	8.3	-1.0	22.7	9.1	-4.3 (-3.0)	0.2	1.0	1.5	
		R	0.45	0.37	0.38	0.54	0.51 (0.34)	0.49	0.47	0.19	
		Mean	21.8	12.2	30.4	21.0	21.3 (31.8)	11.2	10.3	11.3	
EDV3		Bias	4.3	-1.6	13.3	8.1	-1.9 (-0.8)	-2.3	-1.6	1.7	
		R	0.44	0.34	0.36	0.52	0.49 (0.31)	0.49	0.52	0.22	
		Mean	13.9	7.5	23.5	13.3	17.7 (28.3)	7.0	7.7	7.7	
KOV5		Bias	-3.6	-6.3	6.4	0.3	-5.5 (-4.2)	-6.5	-4.2	-1.9	
		R	0.44	0.37	0.41	0.52	0.51 (0.39)	0.49	0.51	0.26	
CO		OBS	Mean	835	597	694	636	443 (493)	527	579	655
			Mean	373	389	455	282	175 (210)	206	162	258
	EDV2	Bias	-462	-208	-239	-354	-267 (-283)	-321	-417	-397	
		R	0.24	0.20	0.42	0.30	0.31 (0.30)	0.21	0.09	0.18	
		Mean	374	359	535	282	196 (208)	221	162	256	
	EDV3	Bias	-461	-238	-159	-354	-247 (-285)	-306	-417	-398	
		R	0.22	0.19	0.35	0.31	0.26 (0.33)	0.24	0.10	0.25	
		Mean	355	358	475	305	190 (217)	231	176	266	
	KOV5	Bias	-480	-239	-219	-331	-253 (-276)	-296	-404	-388	
		R	0.27	0.21	0.48	0.29	0.35 (0.36)	0.15	0.10	0.13	

5 1) Urban area, 2) Non-urban area

6 a) Sichuan-Chongqing-Guizhou, b) South Korea, c) Northeastern China, d) Northern China, e) Southeastern China

1 **Table 3.** Comparison of total NO_x, TOL, XYL, biogenic isoprene emissions, and
 2 formaldehyde to NO₂ ratio (FNR) for different emission data sets in each regional box.
 3 The MEGAN biogenic isoprene emissions are equally applied to all simulations using
 4 different emission data. (unit = mol/s for emissions)

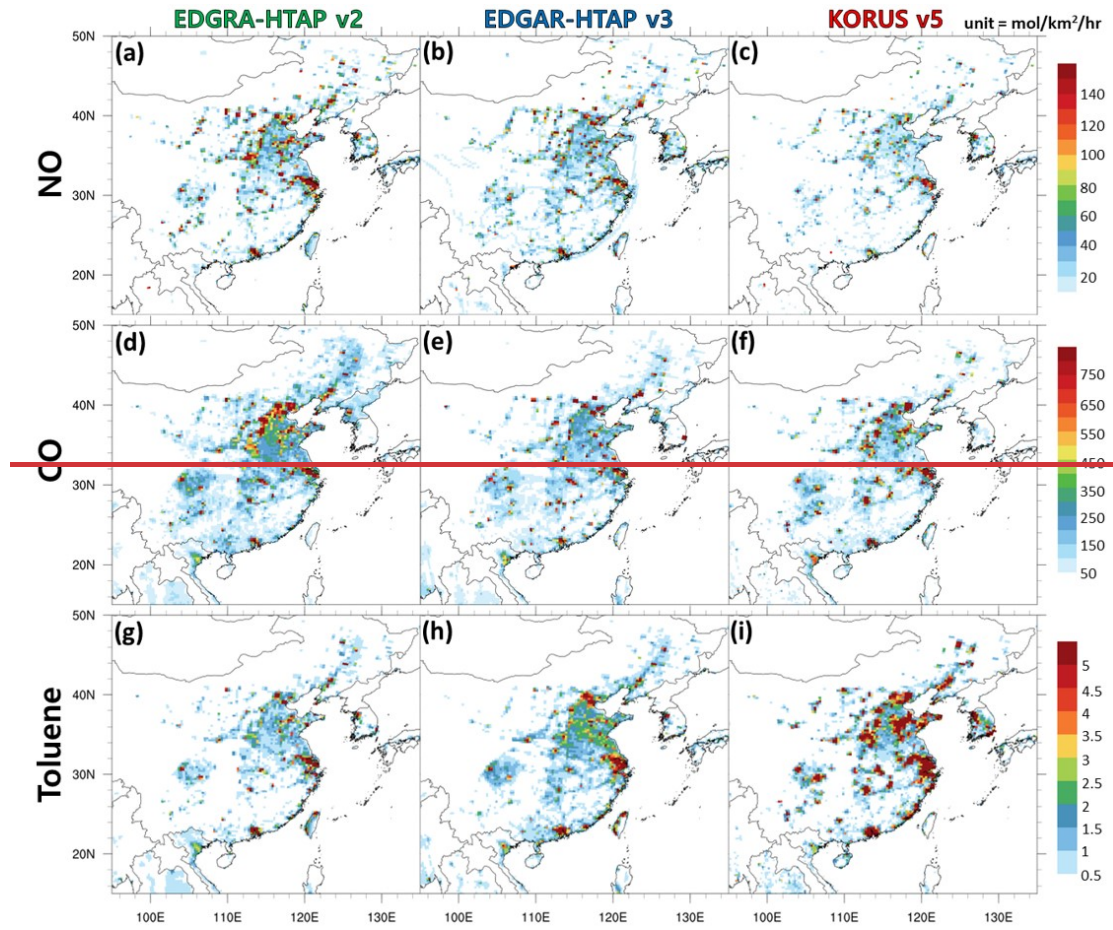
Type	emissions	NCP	SCG	YRD	PRD	KOR(SMA)	NEC	NOC	SEC
<u>NO_x emission</u>	<u>EDV2</u>	5967	1500	2366	1178	990(196)	987	688	590
	<u>EDV3</u>	5202	1654	1642	1091	1191(214)	876	597	662
	<u>KOV5</u>	3237	902	1166	607	886(191)	513	373	410
<u>TOL emission</u>	<u>EDV2</u>	140	56	84	47	27(6)	26	8	20
	<u>EDV3</u>	220	77	99	68	27(8)	40	9	36
	<u>KOV5</u>	403	106	234	155	98(26)	68	21	79
<u>XYL emission</u>	<u>EDV2</u>	84	34	51	28	15(4)	15	4	12
	<u>EDV3</u>	132	46	60	41	16(4)	24	6	22
	<u>KOV5</u>	133	35	79	52	41(9)	21	7	26
<u>Biogenic isoprene emission</u>		132	364	43	127	135(6)	106	23	310
<u>FNR (14-16LT)</u>	<u>EDV2</u>	<u>0.252</u>	<u>1.3122</u>	0.19	0.52	<u>0.532(0.197)</u>	<u>0.6857</u>	0.76	<u>1.1805</u>
	<u>EDV3</u>	0.440	<u>1.3023</u>	<u>0.323</u>	<u>0.524</u>	<u>0.432(0.186)</u>	<u>0.9380</u>	<u>0.944</u>	<u>1.3324</u>
	<u>KOV5</u>	<u>0.7268</u>	<u>2.323</u>	0.48	<u>1.0095</u>	<u>0.71(0.2249)</u>	<u>1.4425</u>	1.49	<u>1.9173</u>

5

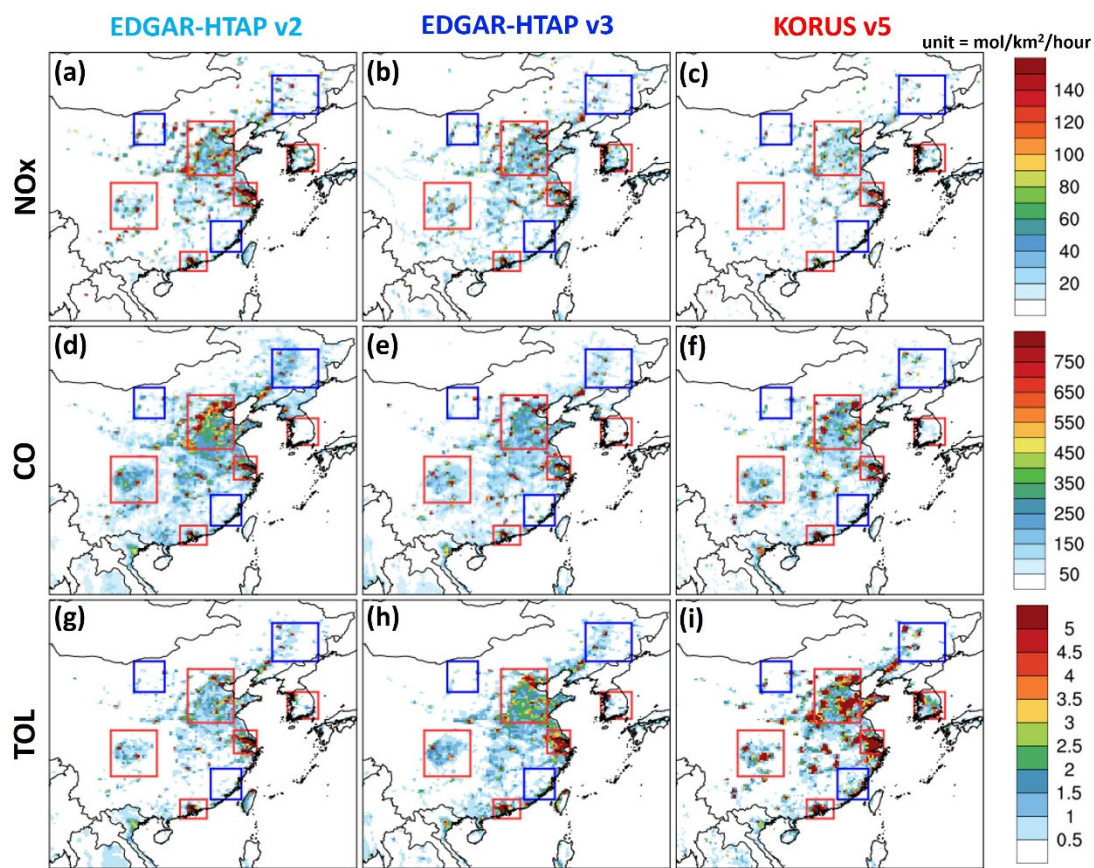
1 **Table 34.** Comparison of aircraft-based 1-minute-interval O₃, NO₂, CO, HCHO, TOL,
2 XYL, ETE, and ISO observations with EDV2, EDV3, and KOV5 for all flight cases
3 under 2 km height (unit = ppb). N is the number of samples. R is correlation coefficient.

Species	Type	N	Mean	Bias	σ	R
O ₃	OBS	5191	84.4		19.9	
	EDV2		67.5	-16.8	16.7	0.44
	EDV3		69.3	-15.1	17.8	0.43
	KOV5		66.9	-17.5	15.8	0.50
NO ₂	OBS	5047	2.19		4.49	
	EDV2		3.06	0.87	4.60	0.71
	EDV3		3.91	1.72	5.34	0.67
	KOV5		2.83	0.64	4.73	0.73
CO	OBS	5575	253		100	
	EDV2		148	-105	48	0.60
	EDV3		156	-97	47	0.59
	KOV5		146	-107	43	0.62
HCHO	OBS	5365	2.37		1.64	
	EDV2		1.75	-0.62	1.01	0.69
	EDV3		1.78	-0.59	1.02	0.67
	KOV5		1.80	-0.57	1.10	0.71
TOL	OBS	730	2.60		2.02	
	EDV2		0.47	-2.13	0.38	0.39
	EDV3		0.55	-2.05	0.48	0.38
	KOV5		1.58	-1.01	1.30	0.37
XYL	OBS	289	0.73		0.65	
	EDV2		0.23	-0.50	0.23	0.30
	EDV3		0.30	-0.43	0.31	0.30
	KOV5		0.49	-0.24	0.47	0.27
ETE	OBS	2573	0.42		1.59	
	EDV2		0.51	0.09	0.65	0.14
	EDV3		0.56	0.14	0.76	0.15
	KOV5		0.51	0.08	0.58	0.20
ISO	OBS	1294	0.08		0.09	
	EDV2		0.18	0.10	0.21	0.41
	EDV3		0.19	0.11	0.20	0.41
	KOV5		0.17	0.10	0.20	0.42

4

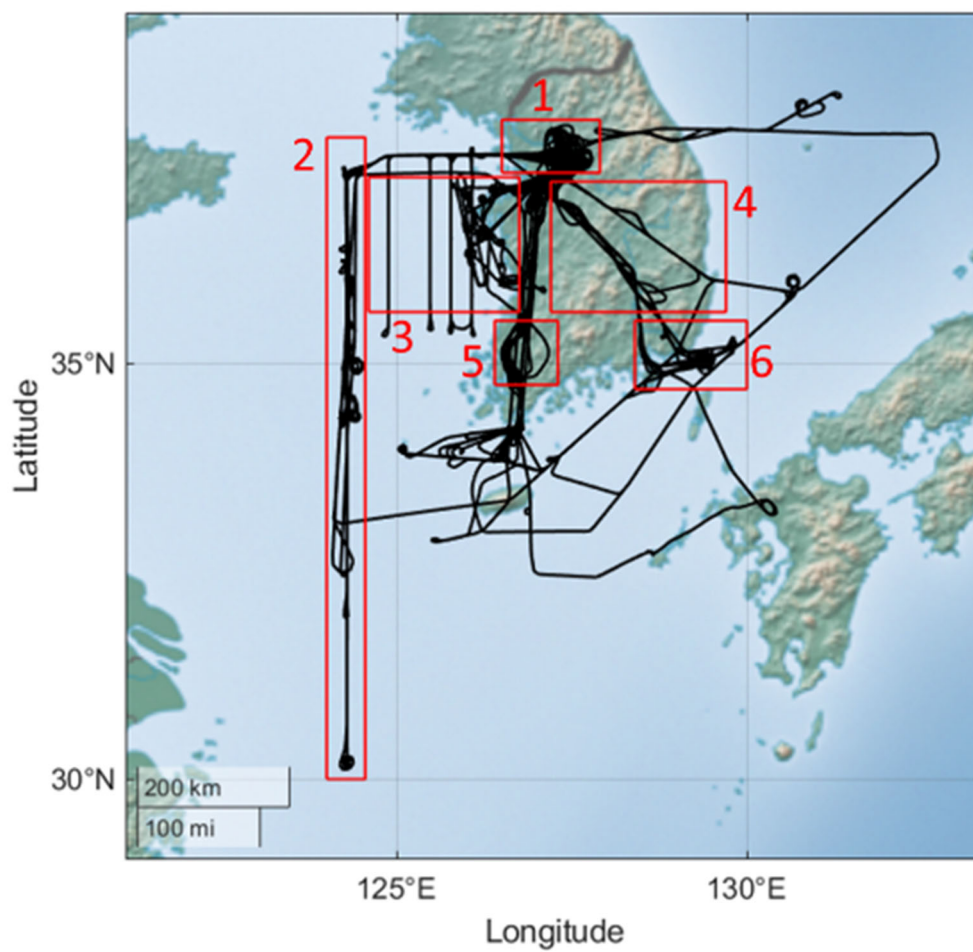


1



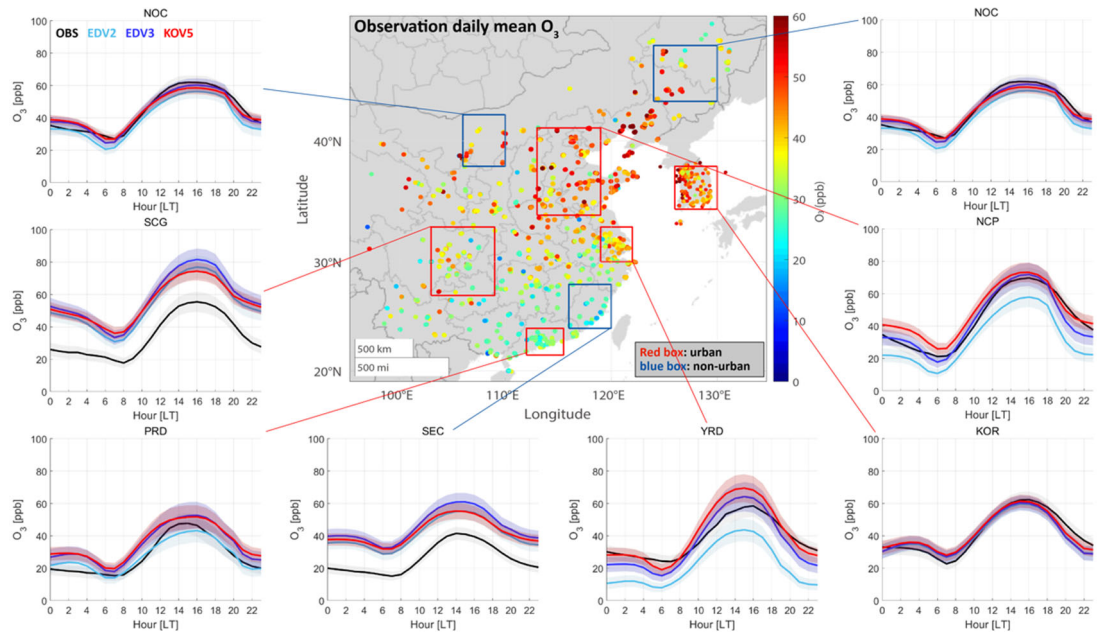
1

2 **Figure 1.** The averaged spatial distribution map of the NO, CO, and TOL (toluene +
 3 less reactive aromatics) emissions from EDGAR-HTAP v2, v3, and KORUS v5 in May.
 4 The boxes represent Northern China (NOC, 38-42°N/106-110°E), Sichuan-Chongqing-
 5 Guizhou (SCG, 27-33°N/103-109°E), Pearl River Delta (PRD, 21.5-24°N/112-115.5°E),
 6 Southeastern China (SEC, 24-28°N/116-120°E), Yangtze River Delta (YRD, 30-
 7 33°N/119-122°E), South Korea (KOR, 34.5-38°N/126-130°E), North China Plain (NCP,
 8 34-41°N/113-119°E), and Northeastern China (NEC, 43-47°N/124-130°E). NOC, NEC,
 9 and SEC are denoted by blue boxes (non-urban). NCP, SCG, PRD, YRD, and KOR are
 10 denoted by red boxes (urban).

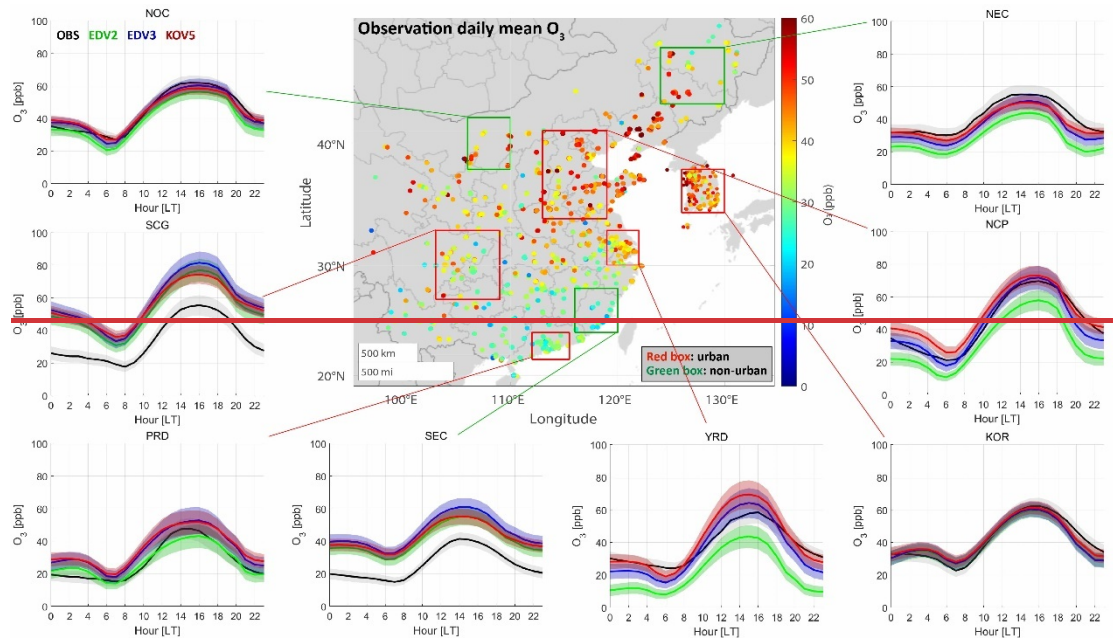


1

2 **Figure 72.** The DC-8 flight paths during the KORUS-AQ campaign period (black) and
 3 6 regional boxes (1: Seoul Metropolitan Area (SMA); 2: Yellow Sea; 3: Chungnam; 4:
 4 Kyungbuk; 5: Gwangju; 6: Busan) (red).

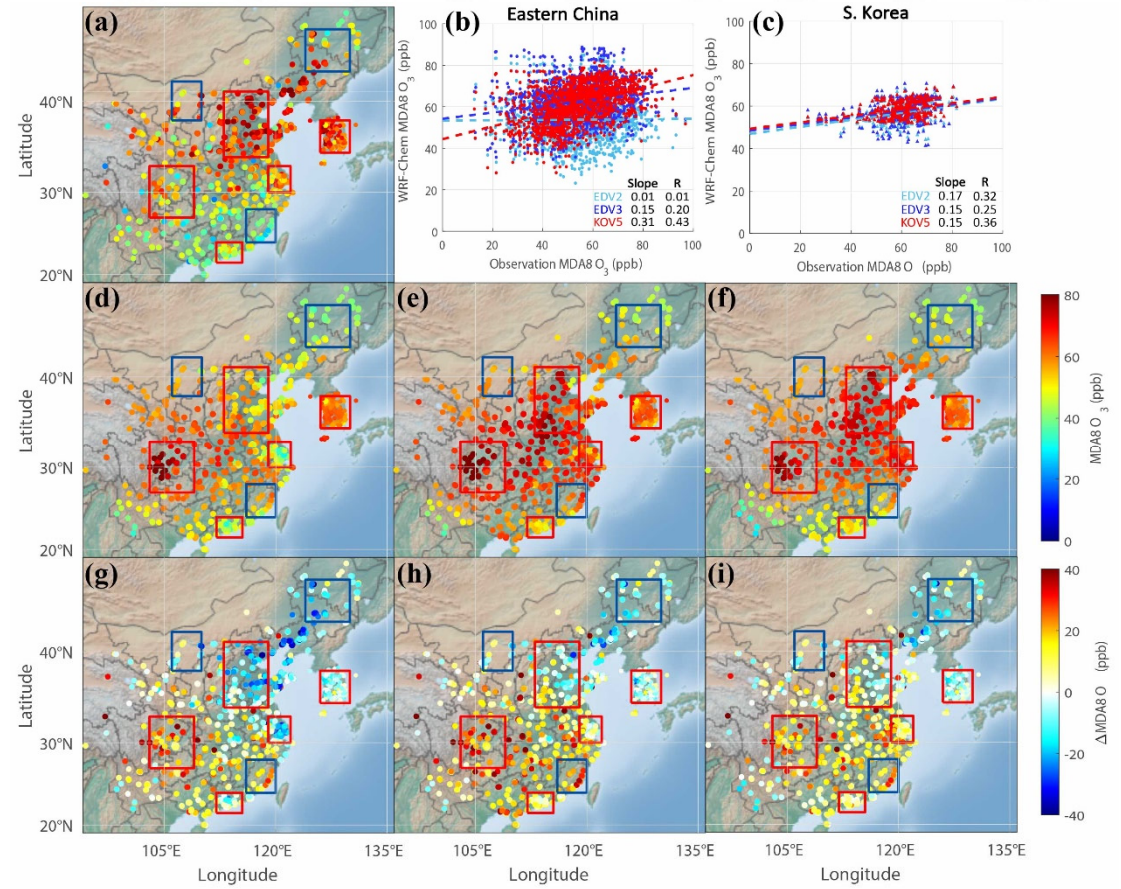
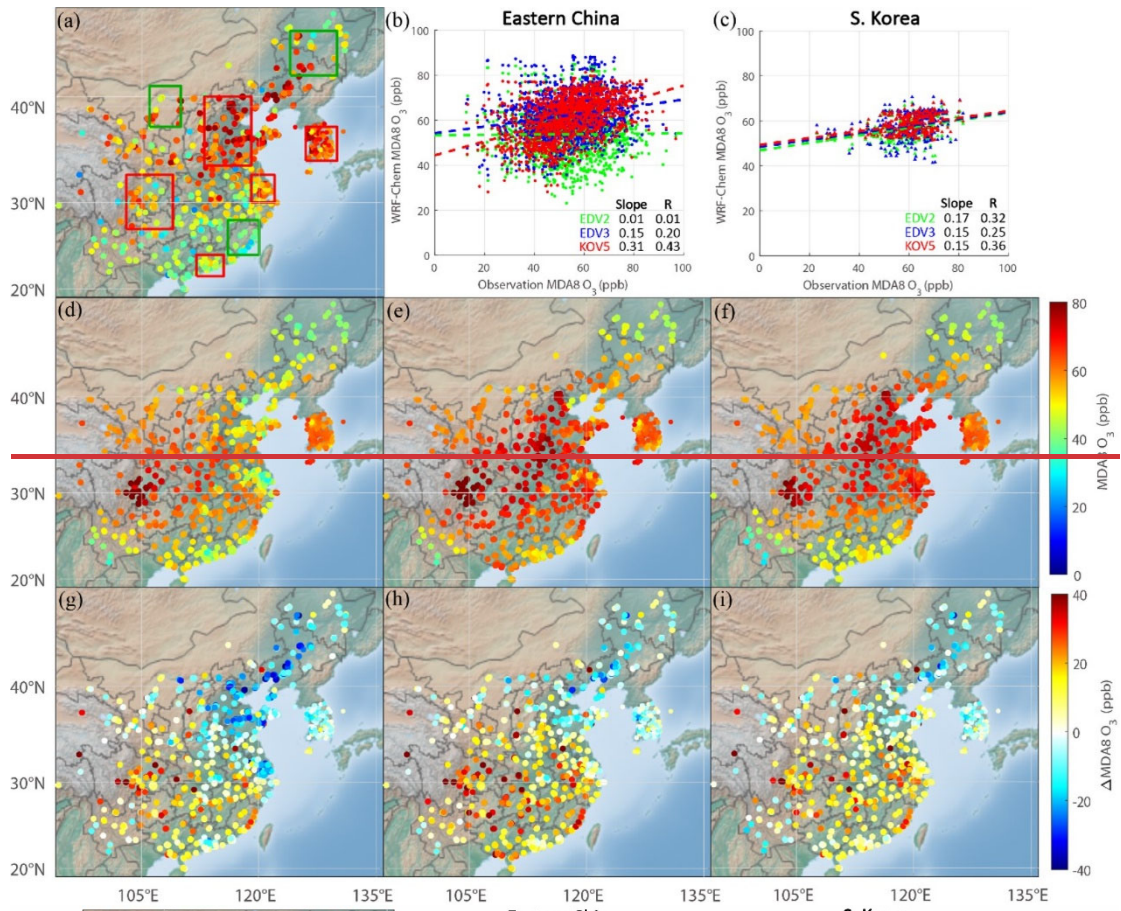


1

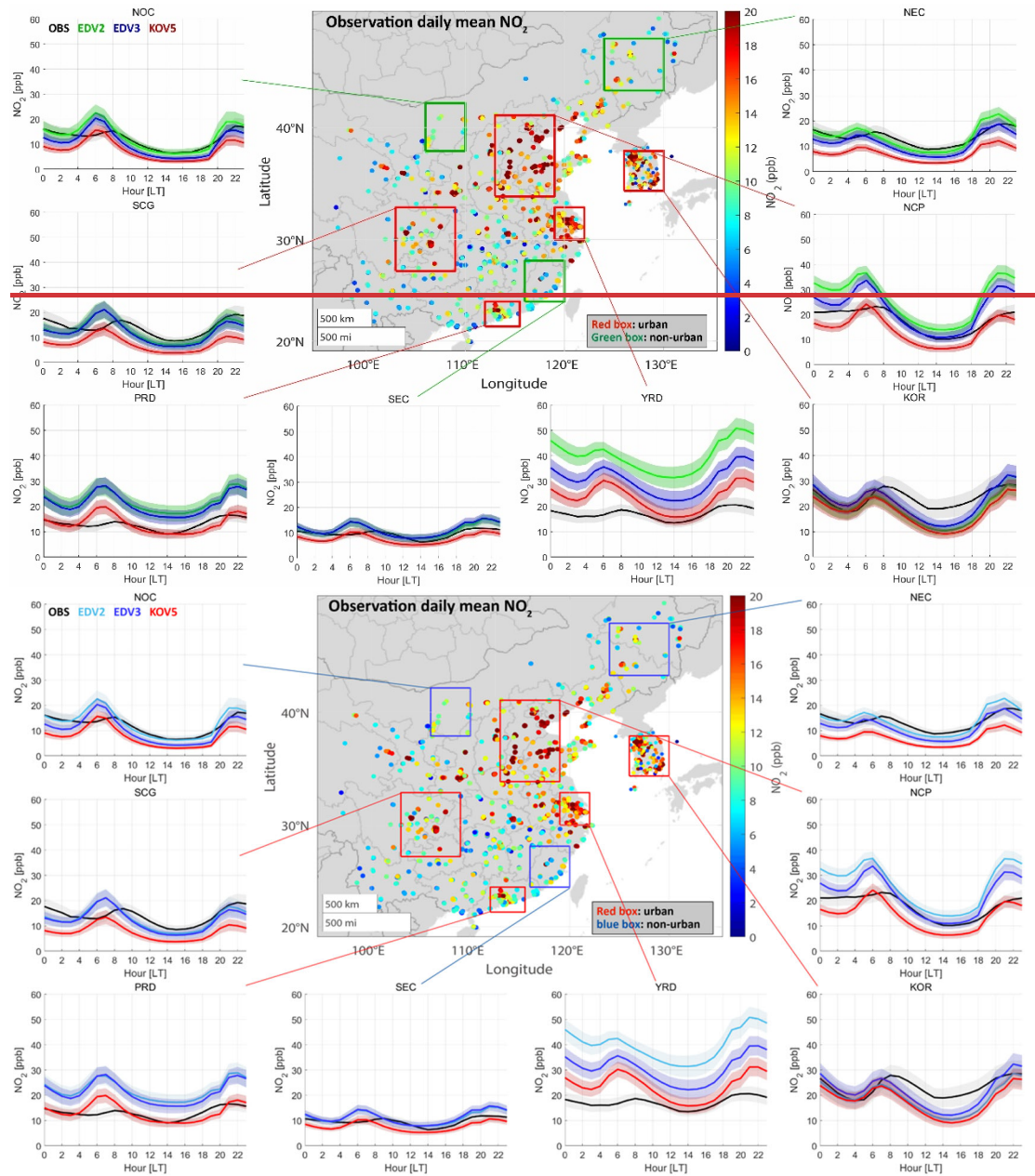


2

3 **Figure 23.** Averaged O₃ concentrations from ground-based observations and model
 4 simulations over the areas that distinguish urban (red box) and non-urban (green box)
 5 region (central plot). Box-averaged diurnal cycle (solid lines) of O₃ and 1/4 of standard
 6 deviations (filled area) from observations (black), EDV2 (greensky blue), EDV3 (blue),
 7 and KOV5 (red) by local time are shown. The results are shown for ~~Northern China~~
 8 (~~NOC, 38–42°N/106–110°E~~), ~~Sichuan-Chongqing-Guizhou~~ (~~SCG, 27–33°N/103–109°E~~),
 9 ~~Pearl River Delta~~ (~~PRD, 21.5–24°N/112–115.5°E~~), ~~Southeastern China~~ (~~SEC, 24–~~
 10 ~~28°N/116–120°E~~), ~~Yangtze River Delta~~ (~~YRD, 30–33°N/119–122°E~~), ~~South Korea~~
 11 (~~KOR, 34.5–38°N/126–130°E~~), ~~North China Plain~~ (~~NCP, 34–41°N/113–119°E~~), and
 12 ~~Northeastern China~~ (~~NEC, 43–47°N/124–130°E~~).



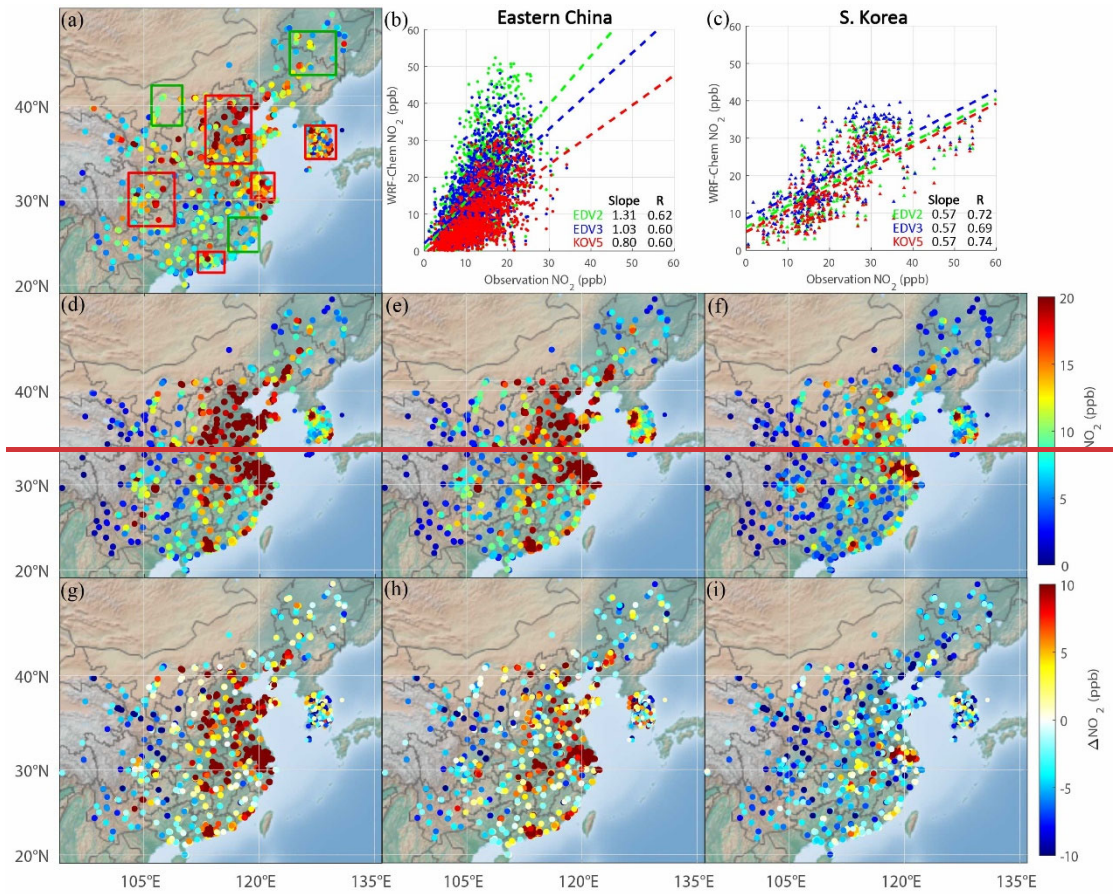
1 **Figure 34.** Comparison of (a) the campaign averaged ground-based maximum daily
2 average of 8-hour O₃ (MDA8 O₃) (unit: ppb) observations and WRF-Chem simulations
3 with (d) EDGAR-HTAP v2 (EDV2), (e) v3 (EDV3), (f) KORUS v5 (KOV5) and (g, h,
4 i) the differences between the observations and model results. The sub-regions are
5 presented with red (urban) and green (non-urban) boxes. The scatter plots comparing
6 averaged observations and the three-emission-based WRF-Chem simulations ([greensky](#)
7 [blue](#); EDV2, blue; EDV3, red; KOV5) are shown in (b) and (c) for Eastern China and
8 South Korea, respectively. (a, d-e) Color-filled circles in (a), (d), (e), and (f) represent
9 the averaged MDA8 O₃ for the whole campaign period (1st May to 10th June).



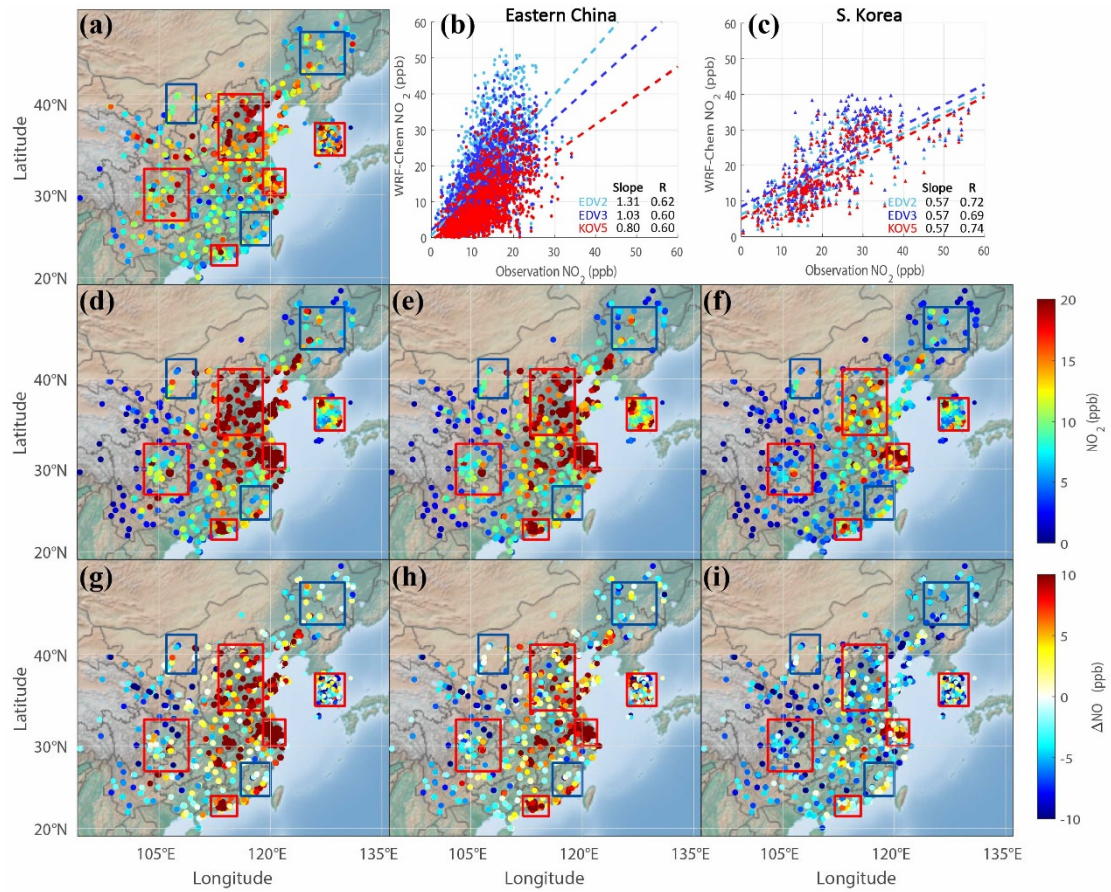
1

2

3 **Figure 54.** The same as **Figure 32** except NO_2 .

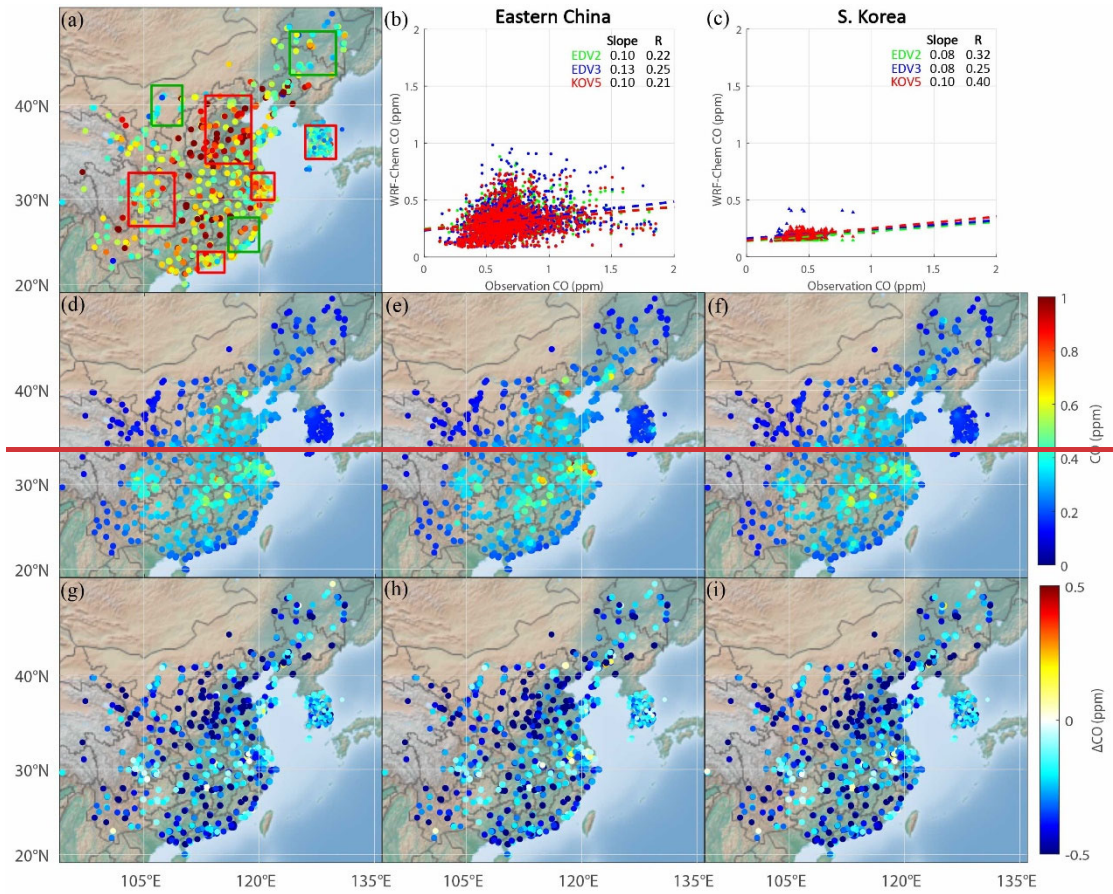


1

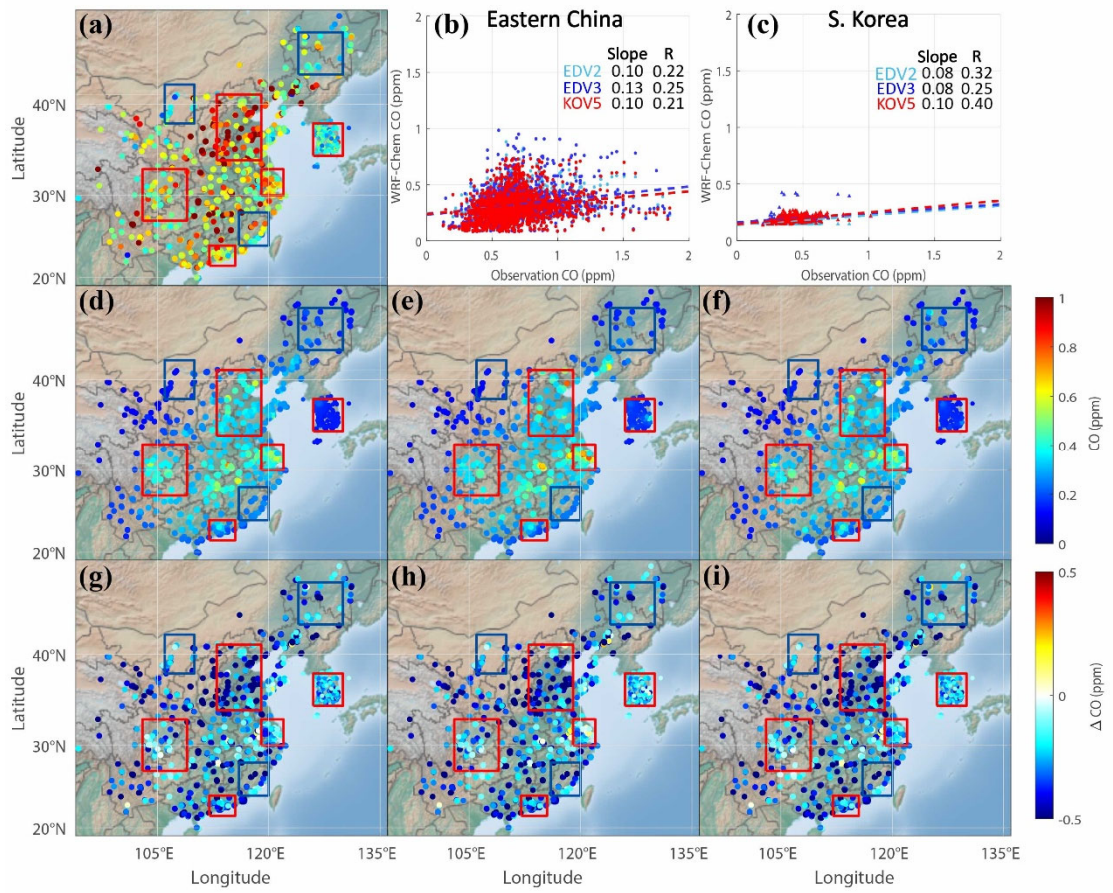


1

2 **Figure 56.** The same as **Figure 34** except daily NO₂ (unit: ppb).

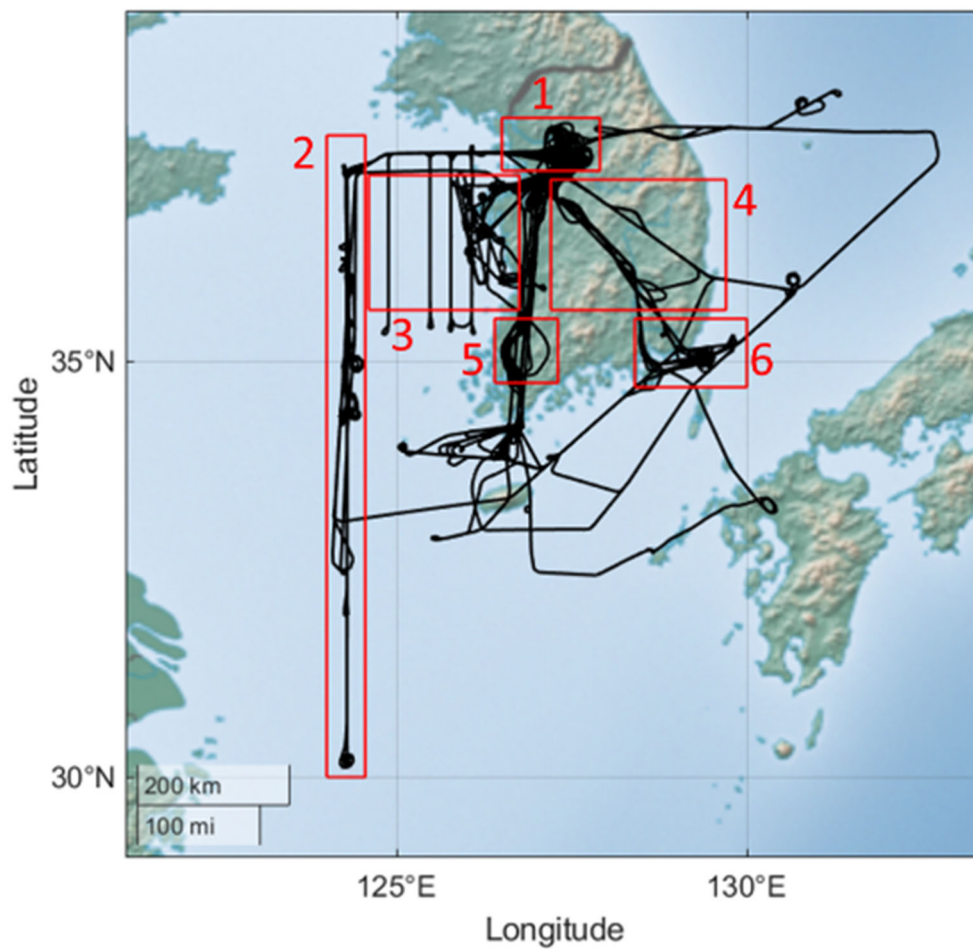


1



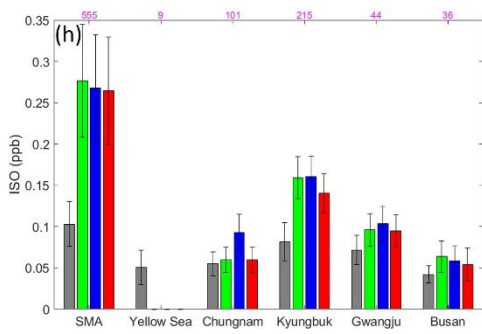
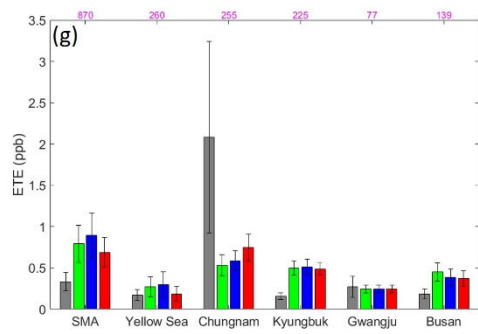
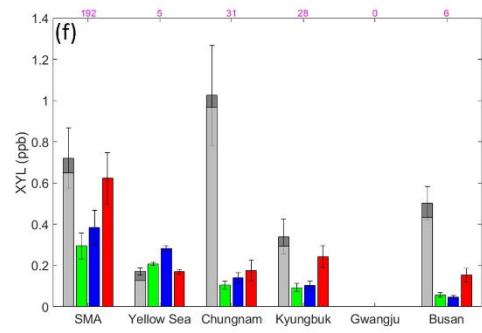
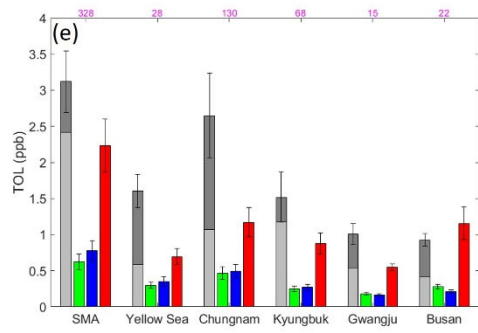
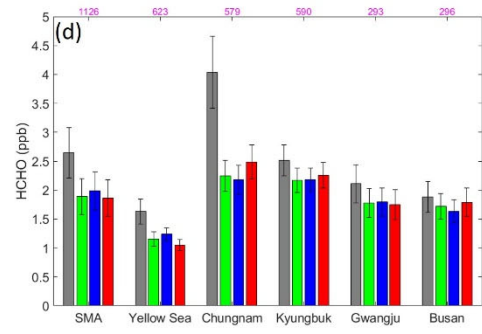
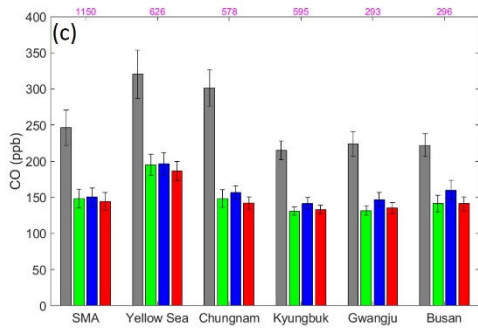
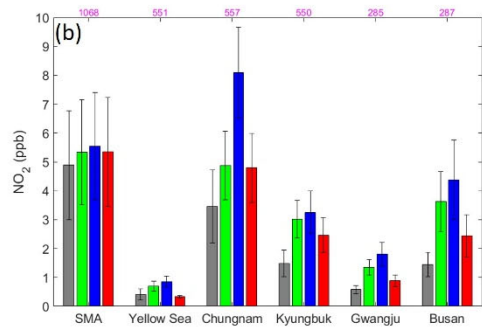
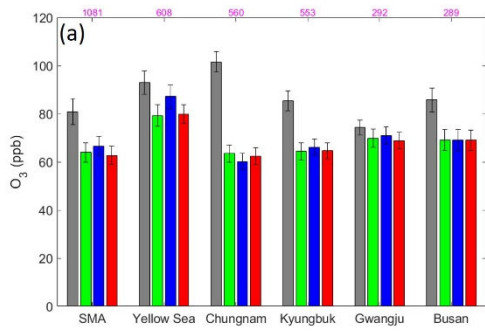
2

1 **Figure 67.** The same as **Figure 34** except daily CO (unit: ppm).

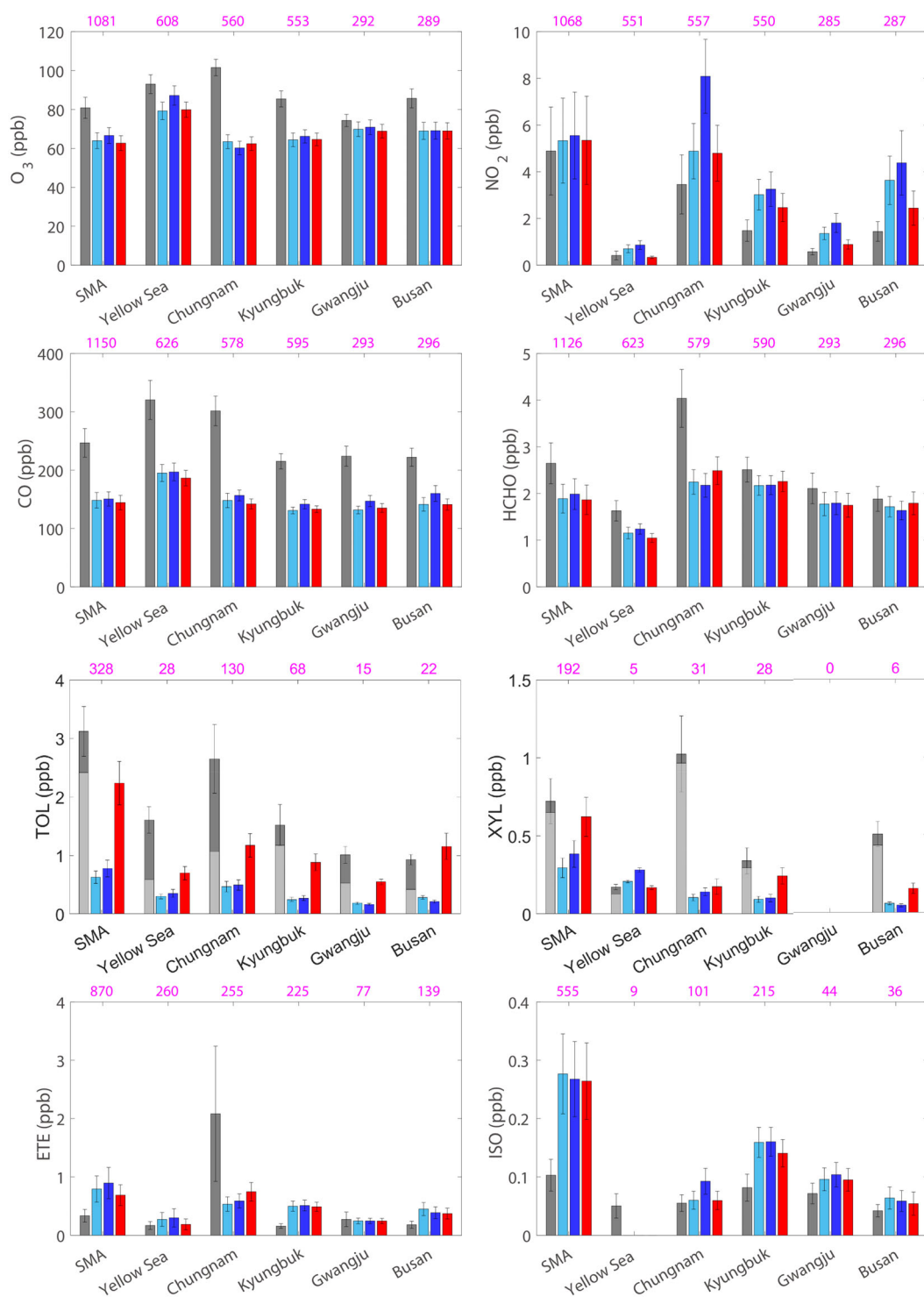


1

2 ~~Figure 7. The DC-8 flight paths during the KORUS AQ campaign period (black) and~~
 3 ~~6 regional boxes (1: Seoul Metropolitan Area (SMA); 2: Yellow Sea; 3: Chungnam; 4:~~
 4 ~~Kyungbuk; 5: Gwangju; 6: Busan) (red).~~

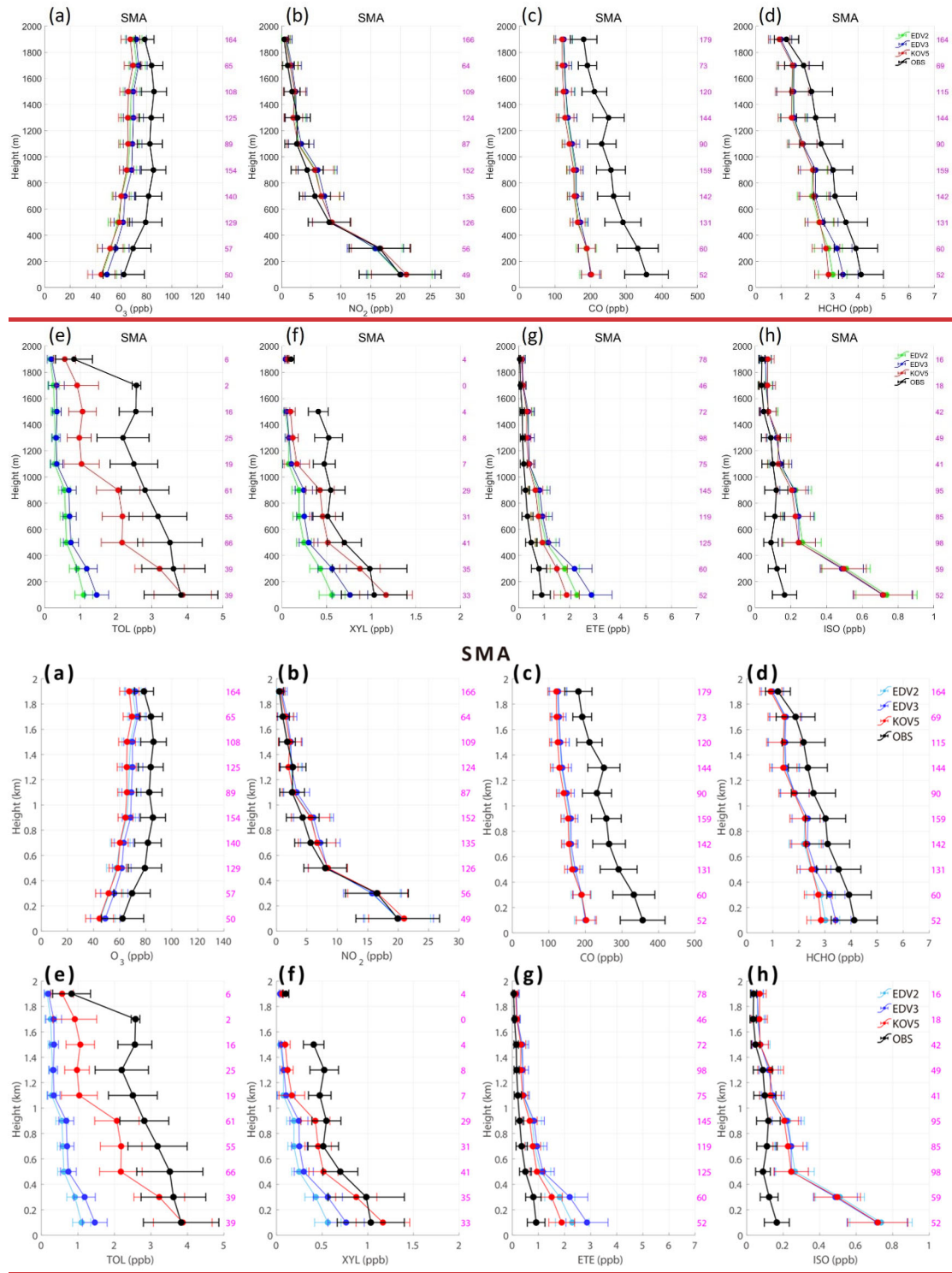


1



1

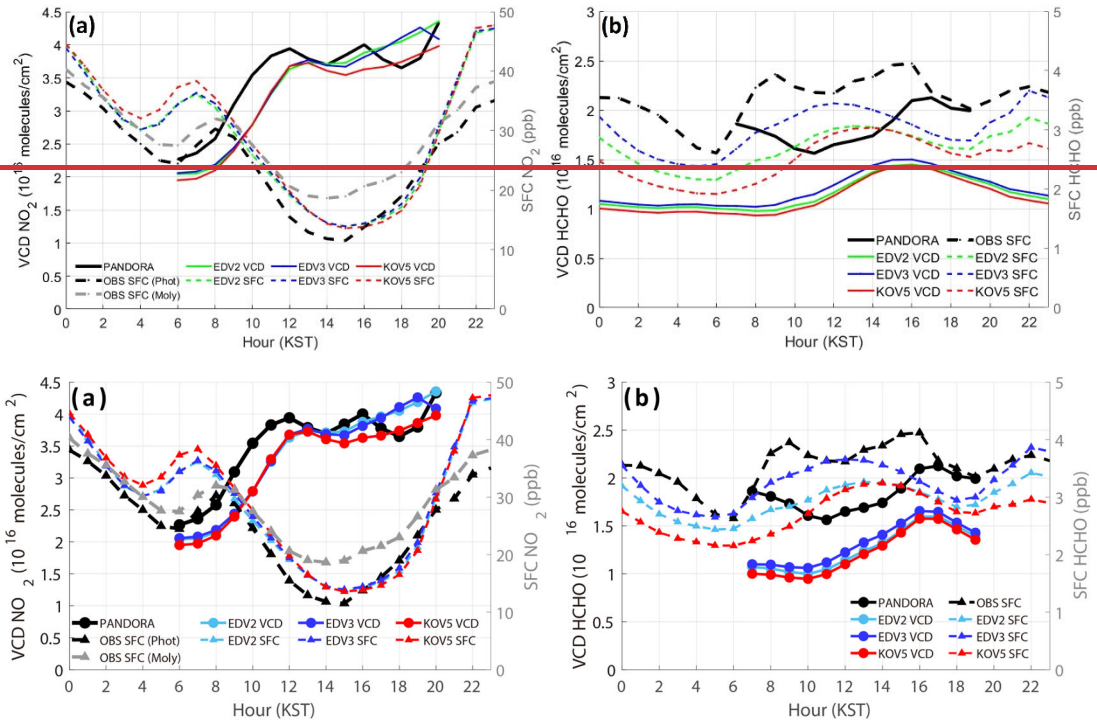
2 **Figure 8.** The mean (bars) and 1/4 of standard deviations (whiskers) of (a) O₃, (b) NO₂,
3 (c) CO, (d) HCHO, (e) TOL, (f) XYL, (g) ethene (ETE), and (h) isoprene (ISO) (unit =
4 ppb) from DC-8 (dark grey), EDV2 (greensky blue), EDV3 (blue), and KOV5 (red) for
5 each box are shown, respectively. TOL and XYL are calculated based on Table S68
6 (Supporting Information). The contribution of toluene to TOL and m/p-Xylene + o-
7 Xylene to XYL is represented with light grey bars (e, f). The sampling numbers are
8 represented with magenta color above the plots.



1

2

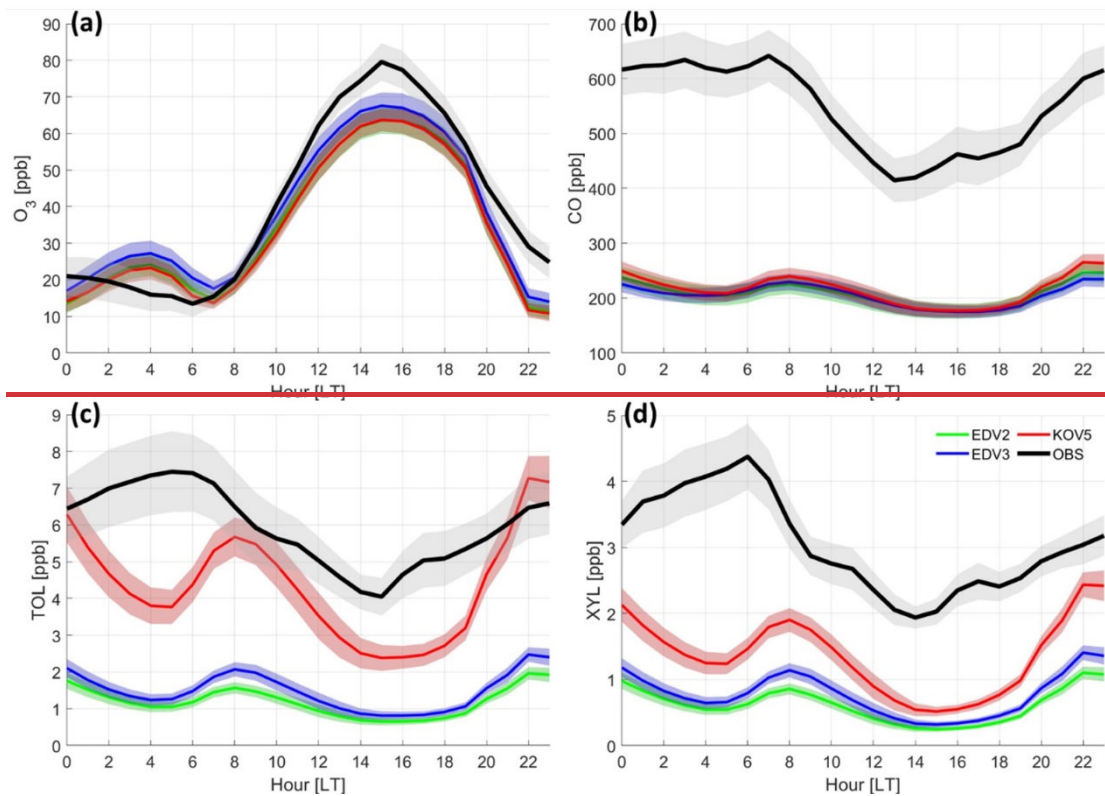
3 **Figure 9.** Vertically averaged (a) O₃, (b) NO₂, (c) CO, (d) HCHO, (e) TOL, (f) XYL,
 4 (g) ETE, and (h) ISO from DC-8 (black), EDV2 (greensky blue), EDV3 (blue), and
 5 KOV5 (red) in SMA under 2 km height above ground level. The 1/2 of standard
 6 deviations are represented with black whiskers in each 200m layer. The sample number
 7 is presented with magenta color on the right side of the plots.



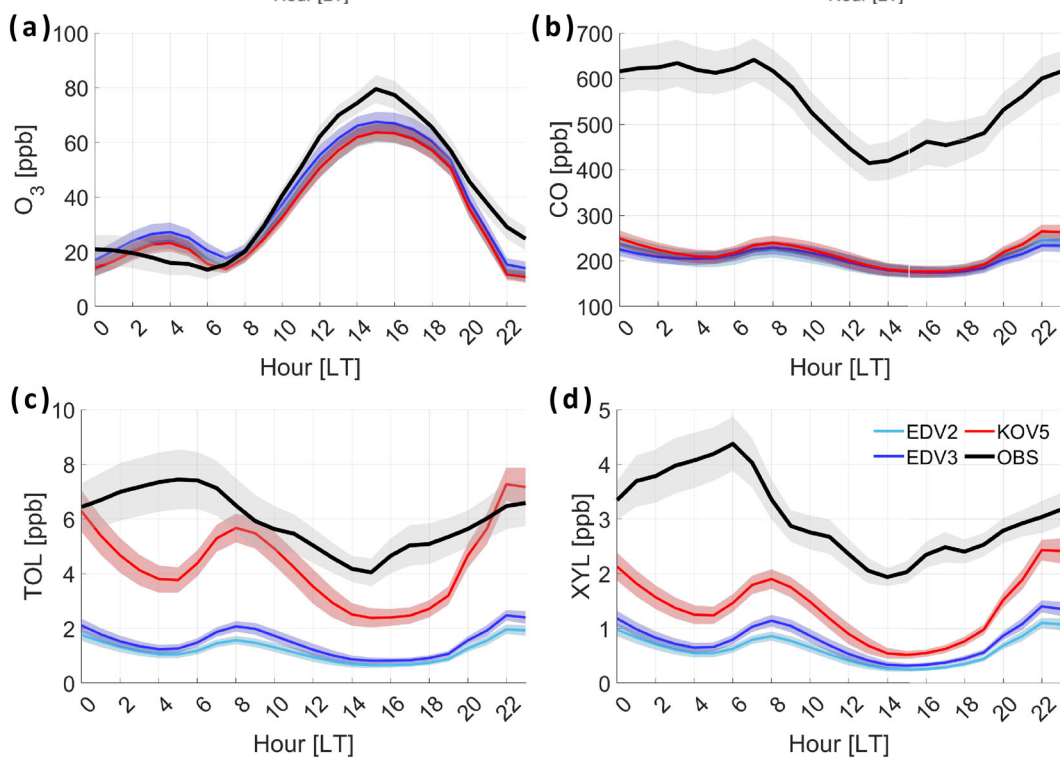
1

2

3 **Figure 10.** The diurnal cycles of vertical columns and surface concentrations of (a) NO₂
 4 and (b) HCHO from Pandora spectrometer (column), and ground-based instruments
 5 (TEI 42i NO_x analyzer and Aerodyne QCL) at the Olympic Park site (37.5232°N,
 6 127.126°E). Surface concentrations of NO₂ are obtained by the two methods:
 7 molybdenum converter and photolytic method. EDV2 (greensky blue), EDV3 (blue),
 8 and KOV5 (red) are compared with observations. The WRF-Chem vertical column
 9 concentrations are produced by summing all vertical layers.

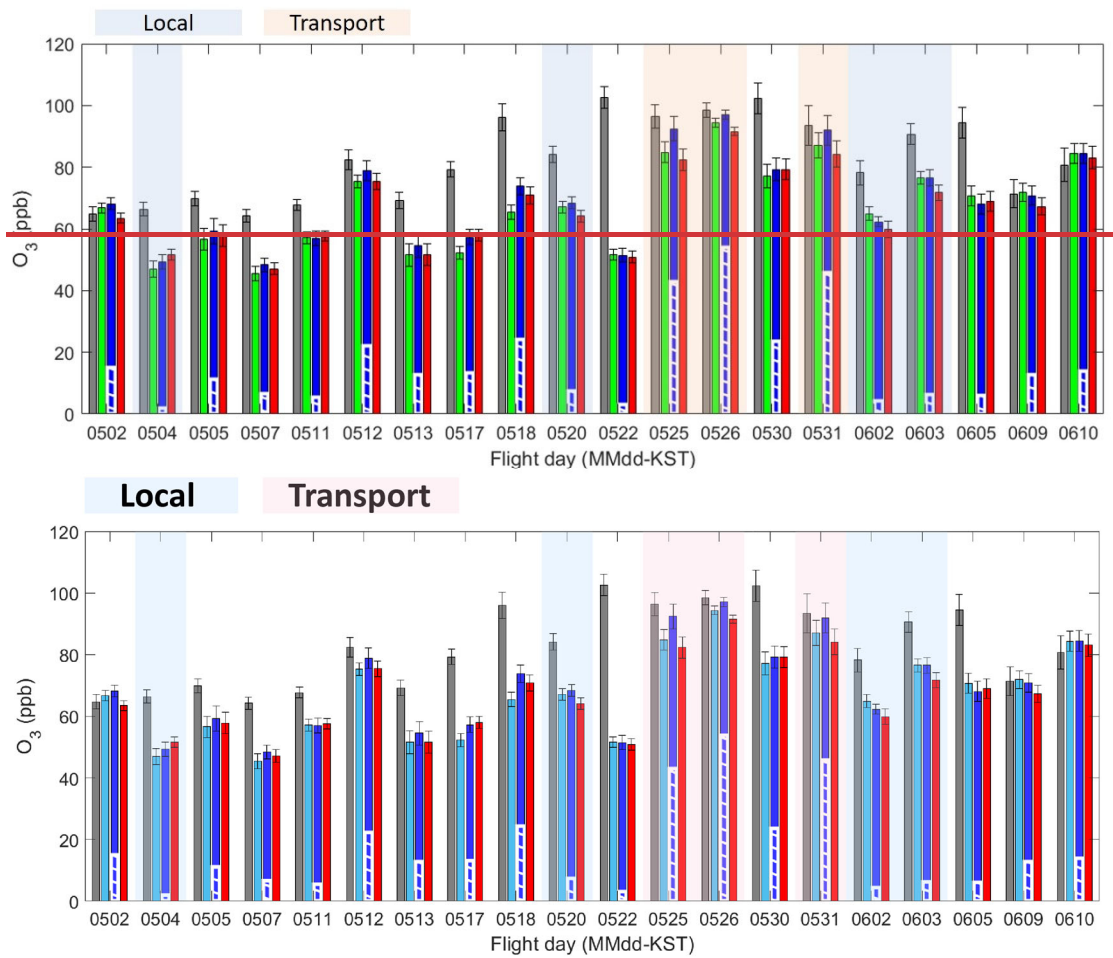


1



2

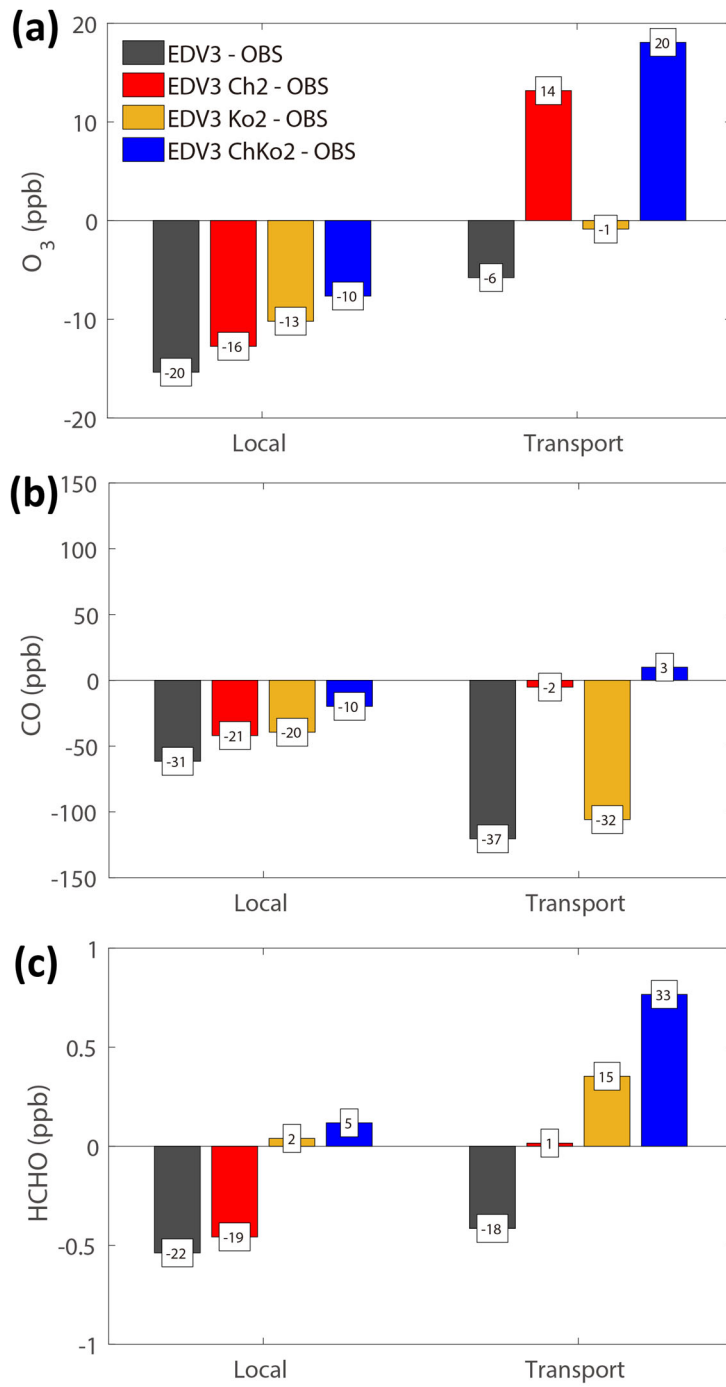
3 **Figure 11.** Diurnal cycles of surface (a) O₃, (b) CO, (c) TOL, and (d) XYL at the
 4 Olympic Park site. EDV2 (greensky blue), EDV3 (blue), and KOV5 (red) are compared
 5 with the observations. 1/4 of standard deviations are represented with grey shades. The
 6 average period is from the 11th May to the 10th June.

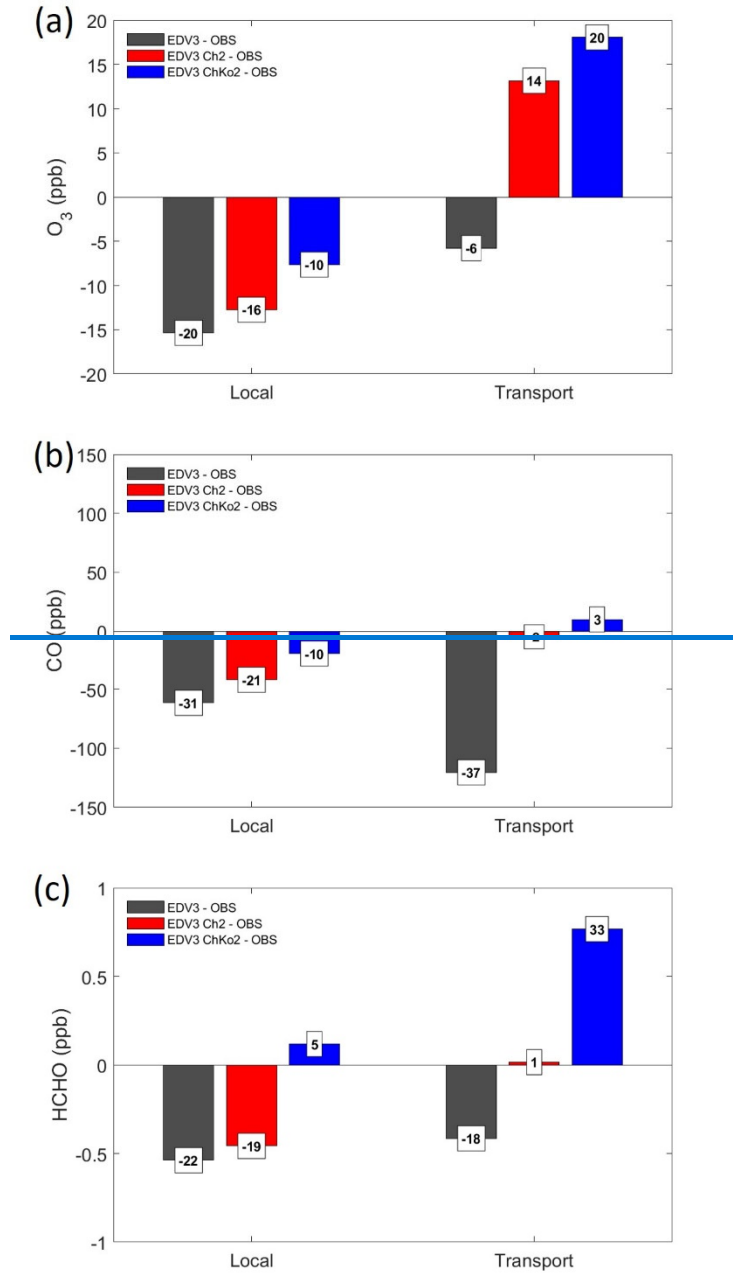


1

2

3 **Figure 12.** Averaged O₃ (bars) and 1/4 of standard deviations (whiskers) (unit: ppbv)
 4 for the 20 DC8 flights (under 2 km height). The observations (grey) are compared with
 5 the model results utilizing EDV2 (greensky blue), EDV3 (blue), and KOV5 (red).
 6 White hatch-filled bars over blue bars are the contribution of Chinese emissions to O₃
 7 concentrations obtained from the default and sensitivity model runs with/without
 8 Chinese anthropogenic emissions. The Local (5/4,20 and 6/2,3) and Transport
 9 (5/25,26,31) cases are shaded with light blue and orange, respectively.



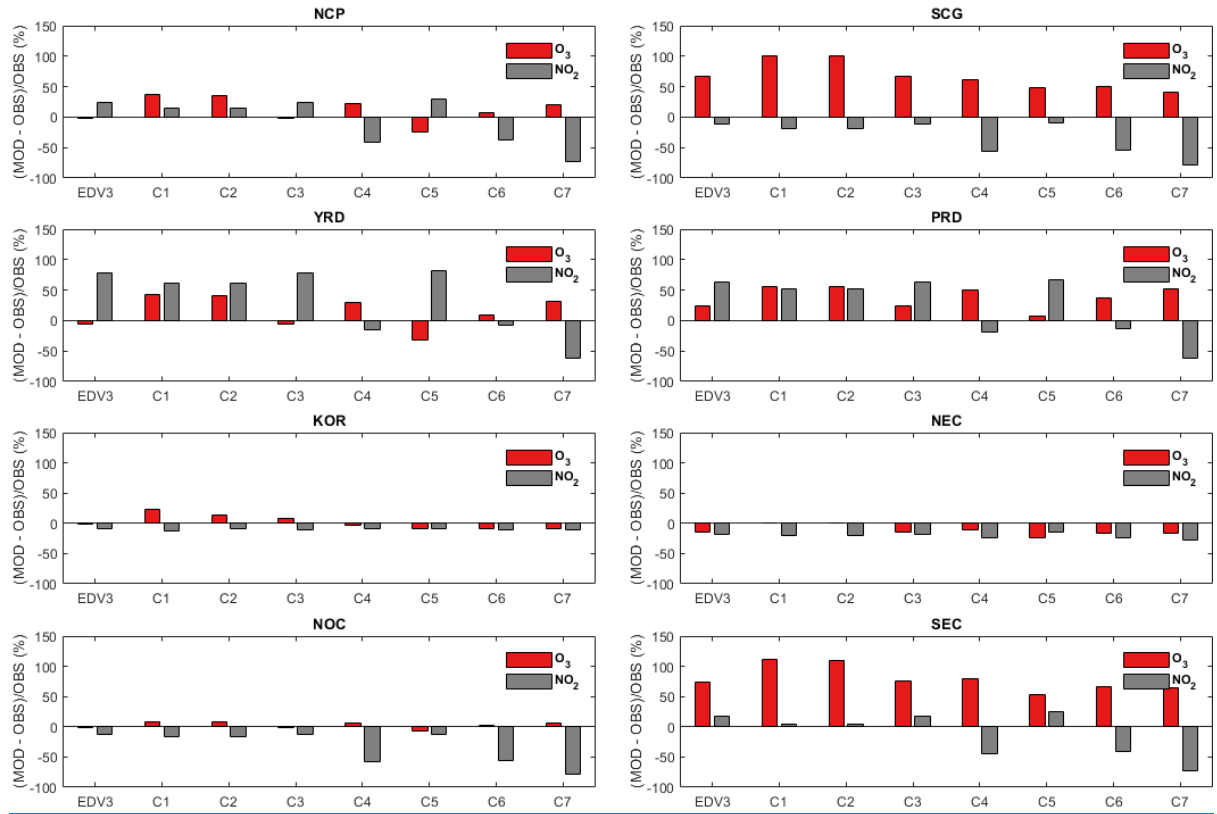


1

2 **Figure 13.** The biases in (a) the model O₃, (b) CO, and (c) HCHO concentrations (bars)
 3 relative to the DC-8 observations under 2 km height over SMA (dark gray: EDV3, red:
 4 EDV3 Ch2, orange: EDV3 Ko2, red: EDV3 ChKo2): (left panel) Local and (right panel)
 5 Transport case. Fractional differences (%) are shown in the white boxes.

1
2
3
4
5
6
7
8

Figure 13. The biases in (a) the model O₃, (b) CO, and (c) HCHO concentrations (bars) relative to the DC-8 observations under 2 km height over SMA (dark gray: EDV3, red: EDV3-Ch2, blue: EDV3-ChK_o2): (left panel) Local and (right panel) Transport case. Fractional differences (%) are shown in the white boxes.

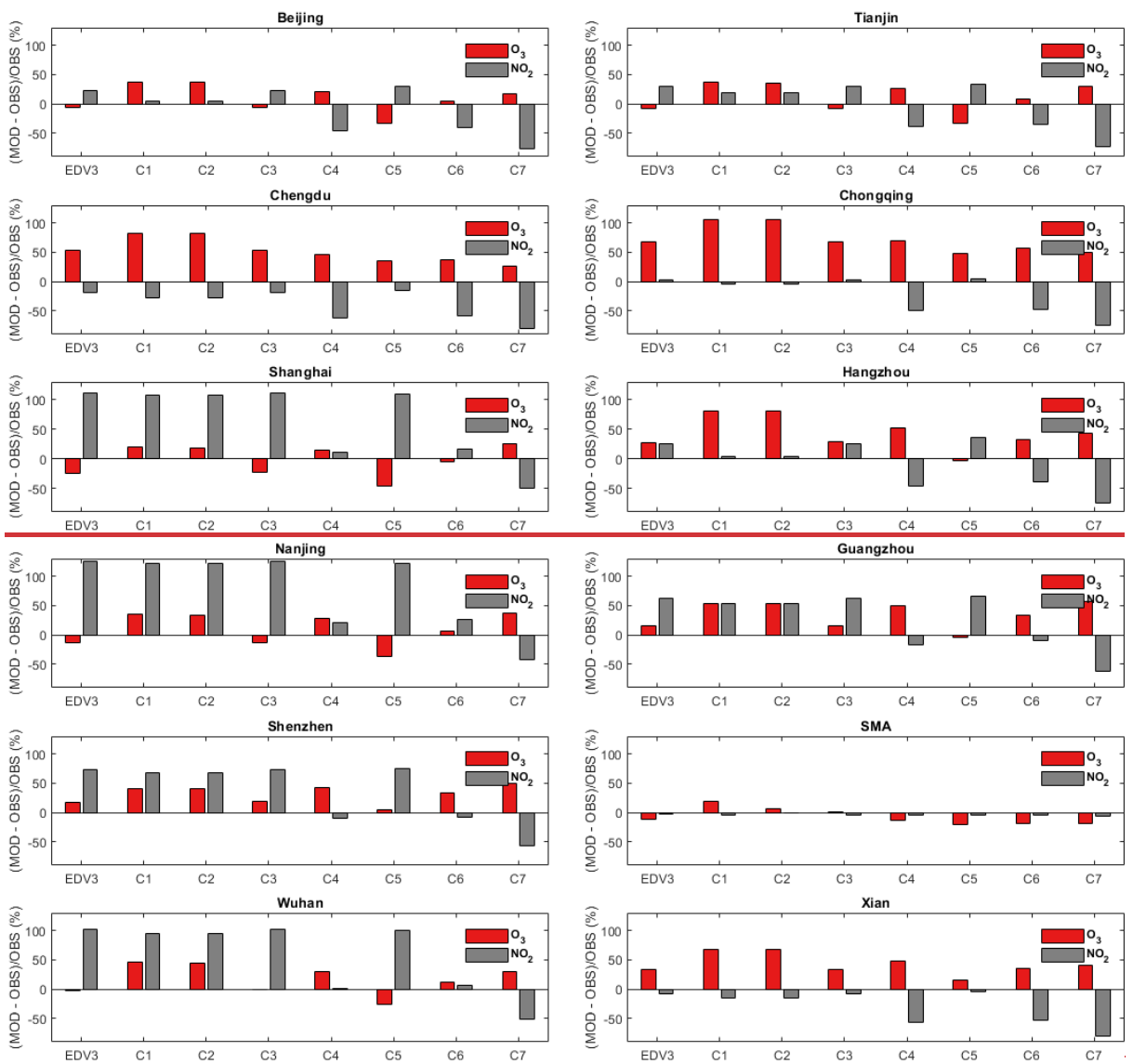


9

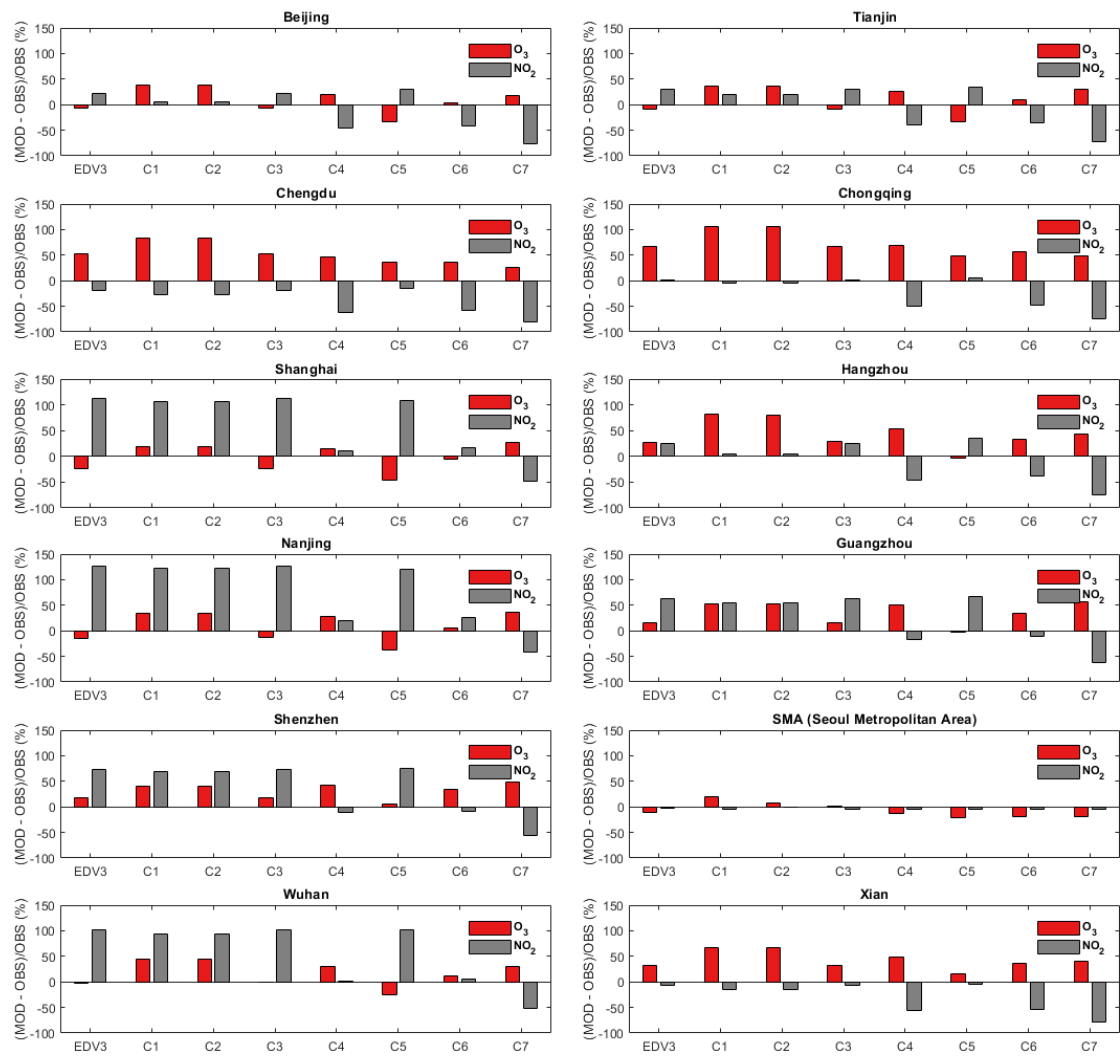
Figure 14. Comparison of relative biases ((Model-Observation)/Observation, unit=%) of daily O₃ and NO₂ at surface observation sites during the KORUS-AQ campaign period from sensitivity simulation (C1-7) with EDV3 in each region (NCP, SCG, YRD, PRD, KOR, NEC, NOC, and SEC). C1; EDGAR-HTAP v3 with double CO and VOC emission in China and South Korea, C2; EDGAR-HTAP v3 with double CO and VOC emission in China, C3; EDGAR-HTAP v3 with double CO and VOC emission in South Korea, C4; EDGAR-HTAP v3 with 50% NO_x reduction in China, C5; EDGAR-HTAP v3 with 50% VOC reduction in China, C6; EDGAR-HTAP v3 with 50% NO_x and VOC reduction in China, C7; EDGAR-HTAP v3 with 75% NO_x reduction in China.

10
11
12
13
14
15
16
17
18

1
2
3
4
5
6
7
8
9



10



1

2 **Figure 15.** Same as **Figure 14** except that the region is changed to cities; Beijing (39.4-
 3 41.1N, 115.4-117.5E), Tianjin (38.55-40.25N, 116.7-118.1E), Chengdu (30.05-31.5N,
 4 103-105E), Chongqing (28.15-32.25N, 105.3-110.2E), Shanghai (30.7-31.5N, 120.85-
 5 122E), Hangzhou (29.2-30.6N, 118.3-120.9E), Nanjing (31.2-32.65N, 118.35-119.25E),
 6 Guangzhou (22.55-24N, 112.9-114.05E), Shenzhen (22.4-22.9N, 113.7-114.65E),
 7 SMA (37.2-37.8N, 126.5-127.3E), Wuhan (29.95-31.4N, 113.65-115.1E), and Xian
 8 (33.65-34.75N, 107.65-109.9E).

9

10

11

12